EVALUATION OF COMPOSITE ALUMINA NANOPARTICLE AND NITRATE EUTECTIC MATERIALS FOR USE IN CONCENTRATING SOLAR POWER PLANTS

A Thesis

by

DARREN ROSS MALIK

Submitted to the Office of Graduate Studies of
Texas A&M University
in partial fulfillment of the requirements for the degree of

MASTER OF SCIENCE

May 2010

Major Subject: Mechanical Engineering

EVALUATION OF COMPOSITE ALUMINA NANOPARTICLE AND NITRATE EUTECTIC MATERIALS FOR USE IN CONCENTRATING SOLAR POWER PLANTS

A Thesis

by

DARREN ROSS MALIK

Submitted to the Office of Graduate Studies of
Texas A&M University
in partial fulfillment of the requirements for the degree of

MASTER OF SCIENCE

Approved by:

Chair of Committee,	Alan Palazzolo
Committee Members,	Debjyoti Banerjee
	Michael Schuller
Head of Department,	Dennis O'Neal

May 2010

Major Subject: Mechanical Engineering

ABSTRACT

Evaluation of Composite Alumina Nanoparticle and Nitrate Eutectic Materials for Use in Concentrating Solar Power Plants. (May 2010)

Darren Ross Malik, B.S., Texas A&M University

Chair of Advisory Committee: Dr. Alan Palazzolo

The focus of this research was to create and characterize high temperature alumina and nitrate salt eutectic nanofluids for use in thermal energy storage (TES) systems. The nitrate eutectic was originally used in the TES system demonstrated as part of the Solar Two power tower and is currently employed as the TES material at Andasol 1 in Spain. Concentrations of alumina nanoparticles between 0.1% and 10% by weight were introduced into the base material in an effort to create nanofluids which would exhibit improved specific heat capacity to reduce the $/kWh$_t$ thermal energy storage system costs.

The composite materials were created using an aqueous mixing method in which both the nanoparticles and nitrate eutectic were placed into solution using acidic water. This solution was then sonicated in an ultrasonic bath in an effort to reduce nanoparticle agglomeration and to improve homogeneity. After boiling off the excess water, the nanoparticle-nitrate eutectic composite was recovered for characterization. The thermal properties of both the composite and base materials were characterized using the differential scanning calorimetry techniques outlined in ASTM E 1269.

The created nanofluids were not stable and did not offer a cost-effective alternative to the current nitrate eutectic TES material. Despite these setbacks, a positive correlation between alumina concentration and nanofluid specific heat was demonstrated. Additionally, the specific

heat capacities of the created nanofluids exceeded that predicted by the current theoretical models. These findings suggest that further work in the field of high temperature nanofluids for use in TES systems is warranted.

DEDICATION

To Erica, without you, I never would have done this.

ACKNOWLEDGEMENTS

I would like to thank my committee chair, Dr. Palazzolo, and my committee members, Dr. Banerjee and Dr. Schuller, for their guidance and support throughout the course of my research. Thanks also go to my friends and colleagues as well as the Mechanical Engineering Department faculty and staff for making my time at Texas A&M University a memorable and rewarding experience. In particular I would like to thank Sandhya Shankar for providing SEM images for my use. I also want to extend my gratitude to the Department of Energy, which provided funding and the foundation for my research. Finally, I would like to thank my parents for their continued love and support.

NOMENCLATURE

α	Thermal diffusivity
ρ	Density
Φ	Volume fraction
ASTM	American Society for Testing and Materials
AverageC_p	Average specific heat of the TES material over the TES operating range
$_{bf}$	Denotes base fluid
°C	Degrees Celsius
C_p	Specific heat capacity
$C_{p,\ Calculated}$	Calculated specific heat capacity
$C_{p,Literature}$	Reference specific heat value
$C_{p,sample}$	Sample specific heat capacity
$C_{p,standard}$	Standard specific heat capacity
CSPP	Concentrating Solar Power Plant
d	LFA sample diameter
D	LFA sample thickness
DOE	Department of Energy
DSC	Differential Scanning Calorimetry
DSC_{ASTM}	DSC signal corrected by Netzsch ASTM algorithm
$DSC_{baseline}$	DSC signal recorded for baseline run
DSC_{sample}	DSC signal recorded for the sample run
$DSC_{sapphire}$	DSC signal recorded for the sapphire run
E	Energy

hr	Hour
HTF	Heat Transfer Fluid
kg	Kilogram
kWh_t	Thermal kilowatt-hour
kWh_e	Electrical kilowatt-hour
LFA	Light Flash Analysis
m	Meter
mg	Milligram
mL	Milliliter
$m_{standard}$	Standard mass
m_{sample}	Sample mass
$_{nf}$	Denotes nanofluid
$_{np}$	Denotes nanoparticle
NREL	National Renewable Energy Laboratory
Q	Energy of LFA flash
$_{Ref.}$	Denotes reference
s	Second
$_{Sample}$	Denotes sample
SEGS	Solar Electric Generation Station
SEM	Scanning Electron Microscopy
t	Time
TES	Thermal Energy Storage
TG	Thermal-Gravimetric
T_H	Highest TES operating temperature

T_L	Lowest TES operating temperature
T_∞	Ambient temperature
ΔT	Change in temperature (T_H-T_L)
V	Volume

TABLE OF CONTENTS

Page

LIST OF FIGURES

FIGURE Page

FIGURE Page

LIST OF TABLES

1. INTRODUCTION: BACKGROUND AND MOTIVATION

On May 9, 1979, President Carter celebrated the installation of a solar-thermal water heater at the White House as a small part of the "greatest and most exciting adventure ever undertaken by the American people" aimed at providing cheap, efficient energy from the Sun [1]. Despite these lofty claims thirty years ago, solar power is currently responsible for less than 1% of the total energy generation in the United States. However, higher fuel prices coupled with an increased demand for energy independence and a desire to mitigate the effects of greenhouse gases and global warming have led the United States to once again consider investing in solar power generation.

The types of commercial concentrating solar power technologies are presented in the following section. Most of these technologies can be coupled with thermal energy storage (TES) systems which allow them to offset their electricity generation to periods of peak demand, smooth out the effects of weather induced transients such as periodic cloud cover, and produce power after the sun has set [2]. The available thermal energy storage technologies are reviewed in Section 1.2. Finally, the developing field of utilizing nanometer sized particles to create nanofluids which have enhanced thermal properties is reviewed in Section 1.3.

The coupling of developments in thermal energy storage and nanofluid technologies is the foundation of this academic research which aims to characterize a composite thermal energy storage material based on Hitec-Solar Salt and alumina nanoparticles. The experimental apparatus, procedures, and analyses used to create and evaluate these composite materials are presented in Section 2.

This thesis follows the style of International Journal of Thermal Sciences.

1.1 Methods of Concentrating Solar Power Production

McKinnon describes the four main forms of commercial concentrating solar power production in *A Primer on CSP* [3]. Two of these methods have been demonstrated by the Department of Energy (DOE) and others in pilot concentrating solar power plants (CSPP) or commercial solar electric generation stations (SEGS). California's solar energy generation station SEGS I was a parabolic trough CSPP built in California which used an organic heat transfer fluid (HTF) [4]. Solar Two was a power tower which used a 60-40 sodium nitrate potassium nitrate salt eutectic, commercially available as Hitec-Solar Salt, as the heat transfer fluid. Solar Two also used a direct two tank TES system to extend the plant's operating window and to smooth out transients caused by clouds and other weather phenomenon [5]. The other two technologies, dish Stirling and Fresnel lenses, have not been demonstrated commercially. However, there are plans in the works to build plants based on these technologies [3].

1.1.1 Parabolic Troughs

Parabolic trough concentrating solar power plants are the oldest means of commercial solar power production. As the name implies, parabolic troughs utilize parabolic mirrors to focus sunlight onto a solar receiver which usually consists of a concentric glass tube and stainless steel pipe which contains the heat transfer fluid for the solar field, see Fig. 1. The space between the glass tube and pipe is evacuated to reduce thermal losses from the HTF. Parabolic troughs are usually mounted onto a single axis pivot which allows the mirrors to track the sun as it travels across the sky.

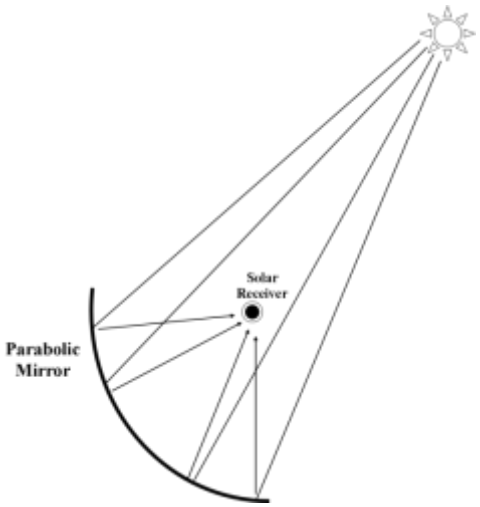

Fig. 1 Two dimensional sketch of the cross section of a parabolic trough solar concentrator.

Parabolic troughs are less efficient than other forms of solar power production because they can only track the sun along a single axis and therefore do not provide correction for seasonal variation in the sun's elevation and path of travel [3]. Additionally, thermal losses from the HTF as it travels along the parabolic troughs limit the length of these solar collectors and ultimately the maximum field temperature. In general, parabolic trough concentrating solar plants have solar fields which operate between 290 °C inlet and 395 °C outlet temperatures.

1.1.2 Central Receivers or Power Towers

Power towers were the second form of commercial concentrating solar power production demonstrated in the United States. Power towers utilize a field of two axis mirrors or heliostats to concentrate the sun's energy onto a central receiver, see Fig. 2.

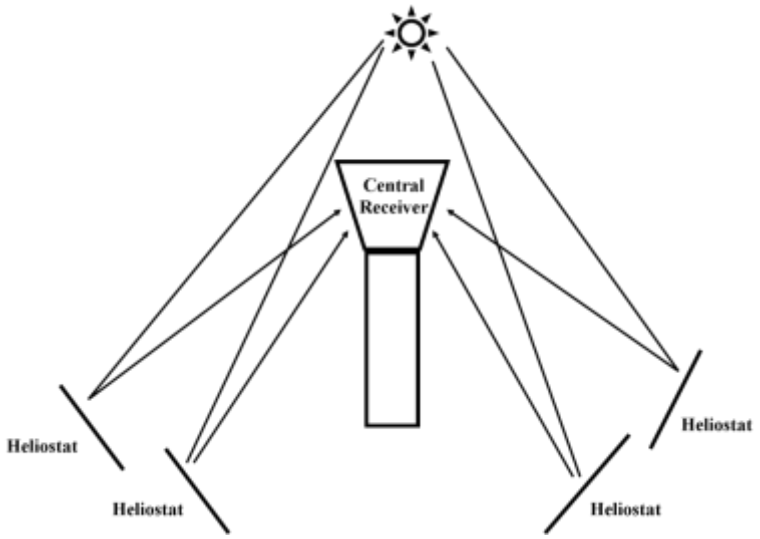

Fig. 2 Sketch of the solar collector and solar concentration components of a solar power tower CSPP.

The central receiver and resulting shorter heat transfer path length allow the HTF to operate at higher temperatures, 288 – 565 °C, and produce higher plant efficiencies than the older parabolic trough technology. The benefits of improved thermal efficiency and lower piping costs are offset by the complexity and cost of the heliostats which pivot along two axes to track the sun as it travels throughout the day [3].

1.1.3 Fresnel Lenses

Fresnel lenses have not been commercially demonstrated but are essentially a simplification of the existing parabolic trough technology. Fresnel lenses replace the single parabolic mirror, which is expensive to manufacture, with a group of linear mirrors which are angled to focus light onto a single receiver similar to that used in parabolic trough plants, see Fig. 3.

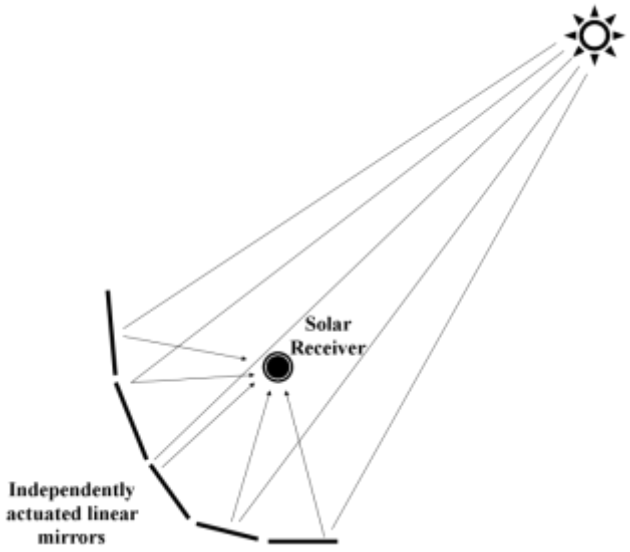

Fig. 3 Two dimensional sketch of a Fresnel lens solar concentrator.

Like the parabolic trough technology they are based on, Fresnel lens concentrating solar power plants are limited by their inability to track the sun along more than one axis and their long heat transfer paths from the concentrator to the power block [3].

1.1.4 Dish Stirling

Dish Stirling concentrating solar power is different from the other forms of concentration solar power production in that it incorporates the concentration and power technologies into a single stand alone device. The dish Stirling system utilizes a parabolic dish to concentrate solar energy onto a receiver, which provides the energy needed to drive an integrated Stirling engine, as shown in Fig. 4. This allows CSPP's which utilize this technology to be "modular" and add generation capacity as demand for electricity increases. The parabolic dishes can be mounted onto two axis tracking devices which allow them to follow the sun precisely as it travels across the sky [3].

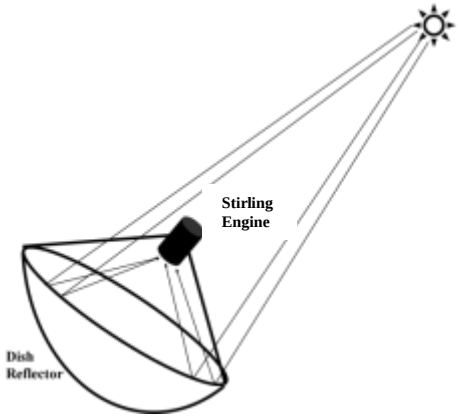

Fig. 4 Sketch of a dish Stirling solar concentrator.

Additionally, the concentration technology can be used to produce very high receiver temperature, 750 °C, which increases the thermal efficiency of the Stirling cycle used to produce electricity. Currently, a dish Stirling system built by Sandia National Labs holds the record for the highest source-to-grid conversion efficiency of any concentrating solar power technology [1].

Unlike dish Stirling systems which integrate the concentration and power conversion devices, parabolic trough, power tower and Fresnel lens concentrating solar power plants utilize a separate solar field to provide thermal energy to the HTF, which is then delivered to the power block, where it is used to turn water into steam and drive a Rankine power cycle. Each of the available concentration technologies can be coupled with a thermal energy storage system which allows the plant to offset energy generation from the time of peak solar load, in the early afternoon, to the time of peak demand, in the early evening. Additionally, TES allows solar power plants to continue to produce power under cloudy conditions and can even extend the hours of power generation into the night after the sun has gone down [2]. The classifications and types of thermal energy storage are presented in the following section.

1.2 Thermal Energy Storage

The concept of thermal energy storage is rather simple: take thermal energy (heat) from the solar field and divert it from the power block to heat up or change the phase of a secondary media to store the thermal energy for later use. Thermal energy storage systems can be classified as direct or indirect systems, which are also categorized as sensible or latent heat storage systems depending on how the thermal energy is stored. Each of these systems allow concentrating solar power plants to smooth out transients, offset electricity delivery to the grid to periods of peak demand, and generate electricity after the sun has gone down. A thorough review of the current state of thermal energy storage is available in a report from the National Renewable Energy Laboratory (NREL) *Survey of Thermal Energy Storage for Parabolic Trough Power Plants* released in 2000 [6]. A brief summary of this report and supporting literature is presented in the following sections.

1.2.1 Classification of Thermal Energy Storage Systems

Traditionally, thermal energy storage systems have been characterized by their method for storing thermal energy. The broad categories of TES systems are sensible heat TES systems, latent heat TES systems, and chemical energy TES systems. Sensible heat TES systems store energy by heating up the TES material. Energy is then recovered as the TES material is allowed to cool. These types of systems are called sensible heat TES systems because they rely on the measureable or *sensible* change in the TES material's temperature to store thermal energy.

Latent heat thermal energy storage systems utilize the relatively high energy of fusion required to melt the TES material to store thermal energy. These types of TES systems usually operate over a much narrower temperature range than those of the sensible heat storage systems. Finally, chemical energy storage utilizes the solar field to drive reversible chemical reactions

which store energy in chemical bonds. When a chemical TES system is discharged, the chemical bonds are broken and the thermal energy can be extracted as needed. These thermal energy storage systems are discussed in greater detail in [6]. The materials created during the course of this research were used to investigate the potential impact of high temperature nanofluids on sensible heat thermal energy storage systems. In general, sensible heat thermal energy storage systems rely on large scale temperature swings in the TES material to store thermal energy as governed by Eq. 1. In Eq. 1; E is the amount of thermal energy stored in the system as a function of temperature, M_S is the mass of the energy storage material, C_p is the temperature dependent specific heat of the energy storage material, and T_H and T_L are the highest and lowest operating temperatures of TES system, respectively.

Amount of energy stored in a TES material as a function of temperature

$$E(T) = M_S \int_{T_L}^{T_H} C_p(T) dT \tag{1}$$

Sensible heat TES systems can utilize solids or liquids as thermal energy storage materials. Table 1 was adapted from *Survey of Thermal Energy Storage for Parabolic Trough Power Plants* [6] and lists the operating range and approximate costs, in 1991 dollars, of sensible heat thermal energy materials on a $\$/kWh_t$ basis. Despite ongoing research into developing latent heat and solid media sensible heat TES systems, CSPP's traditionally rely on liquid sensible heat TES systems such as the two tank system employed in Spain at Andasol 1. The table clearly shows why nitrate salt eutectics such as Hitec-Solar Salt were the material of choice for both Solar II and Andasol 1. The low cost and widespread use of this material were the driving factors in selecting Hitec-Solar Salt as the base material for the foundation of this research.

Table 1
Reported sensible heat storage materials and their associated costs [6].

TES Material	Operating Temp. [C]		Media Costs	Media Costs
	T_L	T_H	[$/kg]	[$/kWh$_t$]
Reinforced Concrete	200	400	0.05	1.0
Cast Iron	200	400	5.00	60.0
Silica Fire Bricks	200	700	1.00	7.0
Synthetic Oil	250	350	3.00	43.0
Nitrite Salts (NO_2)	250	450	1.00	12.0
Nitrate Salts (NO_3)	265	565	0.70	5.2
Carbonate Salts	450	850	2.4	11.0

Sensible heat thermal energy storage systems can be classified by their interface with the solar field as direct or indirect thermal energy storage systems. Direct thermal energy storage systems utilize the solar field's heat transfer fluid as the thermal energy storage medium and therefore do not require heat exchangers. Indirect TES systems do not utilize the solar field's HTF to store energy but rather store heat *indirectly* by using a heat exchanger to heat up the TES material. The most common types of sensible heat thermal energy storage systems are the two tank TES system and thermocline TES system. Both of these thermal energy storage systems can be implemented as direct or indirect systems and are discussed in greater detail in the following section.

1.2.2 Description of Sensible Heat TES Designs

1.2.2.1 Two Tank Storage

Two tank storage systems can be implemented in both direct and indirect configurations. The two tank TES system used at Solar II was implemented as a direct TES system as shown Fig. 5.

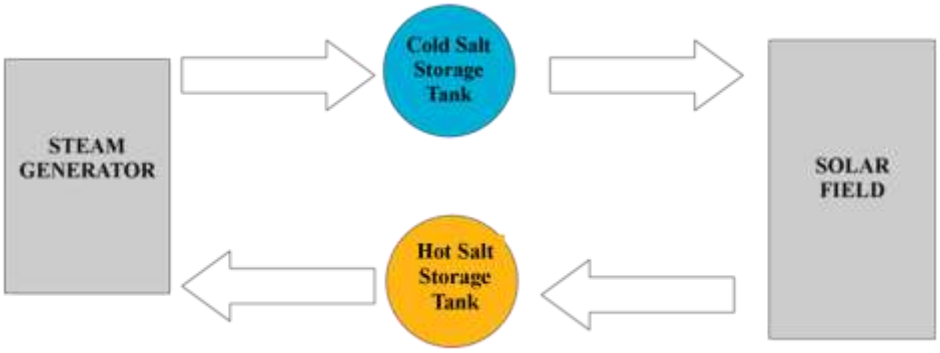

Fig. 5 Schematic of a direct two tank TES system.

As the name implies, two tank TES systems utilize two large isothermal storage tanks. As the system is charged, salt stored in the cold tank is pumped through the solar field or into a heat exchanger where it is heated to its upper operating temperature. The hot salt is then stored in a second salt storage tank until it is needed. When the system is discharged, salt from the hot tank is pumped from the hot tank to the steam generator where it releases its stored energy. The cold salt is then pumped from the steam generator to the cold storage tank until the system can be recharged and the cycle started again.

1.2.2.2 Thermocline

Thermocline systems rely on thermal stratification of the TES material to store energy in a single tank, as shown by the gradient in Fig. 6.

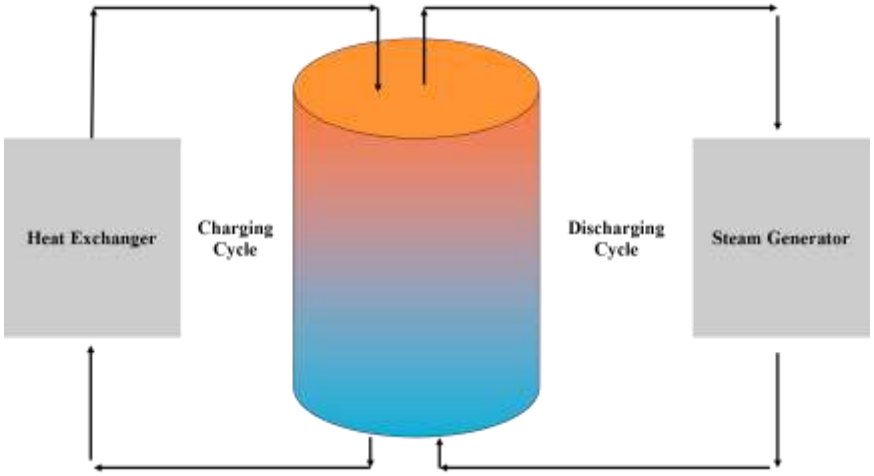

Fig. 6 Schematic of an indirect thermocline TES system.

As the TES is charged, cold liquid is drawn from the bottom of the tank and heated up either directly by the solar field or indirectly in a heat exchanger (as shown); the hot fluid is then reintroduced into the top of the thermocline tank. When the system is discharged, the flow is reversed with the hot fluid being drawn from the top of the tank, is sent to a steam generator where it gives up its thermal energy, and is returned as cold fluid which is pumped into the bottom of the tank. Some thermoclines can be considered hybrid solid/liquid sensible heat storage systems because they utilize a cheap filler material such as limestone, quartz, or sand to replace the more expensive oil or salt heat transfer or TES fluid [7].

This research focused on two tank sensible heat thermal energy storage systems similar to the one employed in the Solar II pilot concentrating solar power plant and the one currently in use at Andasol I in Spain. The two tank system is the simplest of the available sensible heat TES

technologies. Additionally, the purpose of this research is to investigate the ability of alumina nanoparticles to impact the specific heat of Hitec-Solar Salt. Measurement of thermal conductivity is of secondary importance and would need to be investigated thoroughly before the composite was utilized in a thermocline. The effects of thermal gradients on the stability of the composite materials were not investigated. While further study into these effects is needed, the current state of research is best applied to the isothermal cold and hot tanks of the two tank TES system.

1.2.3 Why Thermal Energy Storage

There are several different types of energy storage devices and technologies which could be coupled with concentrating solar power production to extend the power plants delivery of electricity into the evening following sunset. An advantage of thermal energy storage is that it stores the energy collected in the solar field directly, without the thermal-mechanical-potential energy conversion losses of other systems. These potential energy storage systems rely on water displacement or compressed air to store energy until it is needed later. An alternative to potential energy storage systems are electrical energy storage systems, batteries, which store the solar energy after it has been converted to electricity. These energy storage systems are able to avoid storage penalties due to conversion inefficiencies because they store the energy in its final useable state; however, most of these systems are only able to return 75% of the stored electricity to the grid [8]. The approximate $/kWh$_e$ capital costs for these systems are presented in Table 2. These cost estimates where adapted from Divya's *Battery energy storage technology for power systems-An overview* [8]. A euro to dollar conversion factor of 1.484 was utilized to adapt the values given by Divya to provide a direct comparison to reference thermal energy storage cost estimates.

Table 2
Approximate capital costs for available electricity storage systems [8].

Battery type	Largest Capacity	Approximate Cost [$/kWh$_e$]	
Lead Acid (Flooded Type)	10 MW/40 MWh	74.20	222.60
Lead Acid (Valve regulated)	300 kW/ 580 kWh	74.20	222.60
Nickel Cadmium	27 MW/ 6.75 MWh	296.80	890.40
Lithium Ion		1038.80	1484.00
Vanadium redox	1.5 MW/1.5MWh	534.24	1484.00
Zinc Bromine	1 MW/4 MWh	534.24	1484.00
Metal air		74.20	296.80

The Andasol I TES storage system cost is approximated to be between 32.33-30.88 $/kWh$_t$ [9] or 81.80-85.64 $/kWh$_e$, assuming the 37.75% conversion cycle efficiency in DOE's Excelergy model. The low cost of thermal energy storage makes it competitive with the current battery energy storage systems. In addition to offering a cost effective means of storing thermal energy for later electricity production, TES systems offer a buffer against transient weather conditions which can cause the turbine in solar power plants to without thermal energy storage. The potential for nanofluids to lower the thermal energy storage cost below that of lead acid batteries is discussed in the following sections.

1.3 Nanofluids

Nanofluids are generally defined as suspensions or colloids created by dispersing particles less than 100 nm in size into a base fluid. Nanofluids are the latest attempt to improve the thermal conductivity and heat transfer of liquid media by introducing high conductivity particles into water and other heat transfer fluids. In general, heat transfer fluids offer relatively low thermal conductivities when compared to those of solid metals or metal oxides. The concept of adding solid particles to a liquid base material is not a new one; suspensions of millimeter and micrometer sized particles have been used to try and improve the thermal conductivity and heat transfer properties of various heat transfer fluids. However, these suspensions are generally unstable and have failed to provide the necessary thermal properties and performance required to meet the demands of current heat transfer applications. Unlike previous suspensions, which used larger scale particles, nanofluids have been shown to offer higher thermal conductivity and improved critical heat flux while offering improved suspension stability [10].

1.3.1 Enhancement of Thermal Properties

The process by which nanoparticles improve the thermal properties of base fluids is still not well understood. Many early experiments reported results which were not compatible with available heat transfer theories at the time. However, there is a growing base of knowledge which supports the ability of nanofluids to improve the thermo-physical properties of base heat transfer fluids. In general, nanofluids are believed to offer improved thermal properties because the nanoparticles act as bridges or provide structure between adjacent fluid molecules. What is particularly exciting about nanofluids is the ability of nanoparticles at relatively low concentrations, <1% volume fraction, to change the thermal properties like thermal conductivity of the base fluid by ~10% - 40% [10]. The size and concentration of the nanoparticles in the

nanofluid have been shown to affect the fluid thermal conductivity. Much of the research into nanofluids has focused on efforts to improve the thermal conductivity of the base fluid, while nanofluid specific heat, viscosity, and other thermal and fluid properties have received less attention.

In 2008, a paper by Zhou and Ni entitled *Measurement of the specific heat capacity of water-based Al_2O_3 nanofluid* [11] claimed that the specific heat of water-based nanofluids could be predicted using the model given in Eq. 2. The model predicts the specific heat of a nanofluid, $C_{p,nf}$, based on the density, ρ, specific heat, C_p, of the nanoparticles, np, and base fluid, bf, along with the volume fraction of the nanoparticles, Φ.

Proposed model for predicting the specific heat of nanofluids

$$C_{p,nf} = \frac{\Phi(\rho C_p)_{np} + (1-\Phi)(\rho C_p)_{bf}}{\Phi\rho_{np} + (1-\Phi)\rho_{bf}} \quad (2)$$

The scope of the investigation was rather limited as the average specific heat of the nanofluid was only calculated for a temperature range of 25 - 40 ^{o}C. Despite the limited experimental temperature range, the model was shown to agree quite well with experimental results over a wide range of nanoparticle volume fractions, 0-21.7%. Differential scanning calorimetry (DSC) measurements performed by Zhou showed that the introduction of alumina nanoparticles into water produced nanofluids which exhibited smaller specific heats than that of the base fluid [11].

Previous work at the Air Force Research Lab in the field of nanofluids contradicts the experimental results published by Zhou. Experiments performed by I.C. Nelson showed approximately a 30% improvement in the specific heat of a water-based nanofluid which used exfoliated graphite nanoparticles [12].

The nanofluids created for this research into developing new TES materials are an entirely new class of nanofluids which utilize Hitec-Solar Salt as the base fluid. Due to the exploratory nature of this academic work, alumina nanoparticles were selected as the nanoparticle of choice due to their wide availability and relatively low cost.

1.4 Potential Impact of High Temperature Nanofluids on TES Systems

Andasol 1 in Spain is a CSPP which utilizes parabolic troughs and a two-tank storage system which has the capacity to store enough thermal energy to operate the turbine for 7.5 hours after the solar field has shut down for the day. Due to the geographic location of the plant, Andasol 1 is able to provide electricity almost 24 hours a day during the summer months [2]. In general, larger capacity TES systems require a larger capital investment but deliver energy at a lower cost because the larger capacity allows for increased power production and spreads the cost of the system over a larger operating window [4].

Despite the widespread literature supporting the economics and benefits of coupling thermal energy storage systems with concentrating solar power plants, only four thermal energy storage systems have been constructed in the United States, none of which are in operation today. California's Solar I and Solar II pilot plants were each shut down following the completion of their test periods of operation. The solar energy generation station SEGS I in California had a two-tank TES system that caught fire and was never repaired or replaced. Presumably, the lack of TES systems in the American solar power industry is due to the large capital costs associated with these systems.

The DOE uses a $\$/kWh_t$ figure of merit for evaluating potential thermal energy storage systems when evaluating TES systems. The $\$/kWh_t$ costs of thermal energy storage materials, which operate over a particular temperature range (ΔT), are calculated using Eq. 3. As the

equation shows, any increase in the specific heat or the operating range of the thermal energy system results in an improved $/kWh$_t$ media cost. For the purposes of this research it is assumed that the introduction of nanoparticles will change the operating range, ΔT, of the TES as this will be established by the capabilities of the solar field to heat the HTF to the upper temperature, T_H, while the demands of the power block will establish the lowest temperature, T_L, at which energy can be extracted from the TES. As discussed in the preceding section, the introduction of nanoparticles into Hitec-Solar Salt was meant to produce composite nanofluids which had improved specific heat capacities.

Figure of merit for DOE thermal energy storage media on a [$/kWh$_t$] Basis

$$MediaCosts\left[\frac{\$}{kWh_t}\right] = \frac{MaterialCosts\left[\frac{\$}{kg}\right]}{AverageC_p\left[\frac{kJ}{kgK}\right] \times \Delta T[K] \times 2.778E-4\left[\frac{kWh_t}{kJ}\right]} \quad (3)$$

The purpose of this research was to determine if the introduction of alumina nanoparticles into Hitec-Solar Salt offers a cost-effective improvement in the specific heat of thermal energy storage material. Fig. 7 shows the results of a parametric study into the potential cost benefit of introducing nanoparticles into Hitec-Solar Salt. Four different curves representing 0, 10, 25 and 50% increases in material costs due to the introduction of nanoparticles are plotted as a function of theoretical improvement in the TES materials specific heat. The normalized media costs are plotted as the dependent variable for this parametric study. From the plot, it is possible to determine that a composite material produced at a 10% higher manufacturing cost with a specific heat 1.5 times higher than that of the base Hitec-Solar Salt yields more than a 25% savings with respect to the current Solar Salt TES material. Similarly, a new TES material which demonstrated a 30% increase in specific heat similar to that observed by Nelson would offer a

15% savings if it could be produced at only a 10% higher material cost. If the cost of producing the material were to increase by 30% or more, there would be no advantage to the new material. The predicted cost increase for each of the measured mass concentrations is given in Table 3.

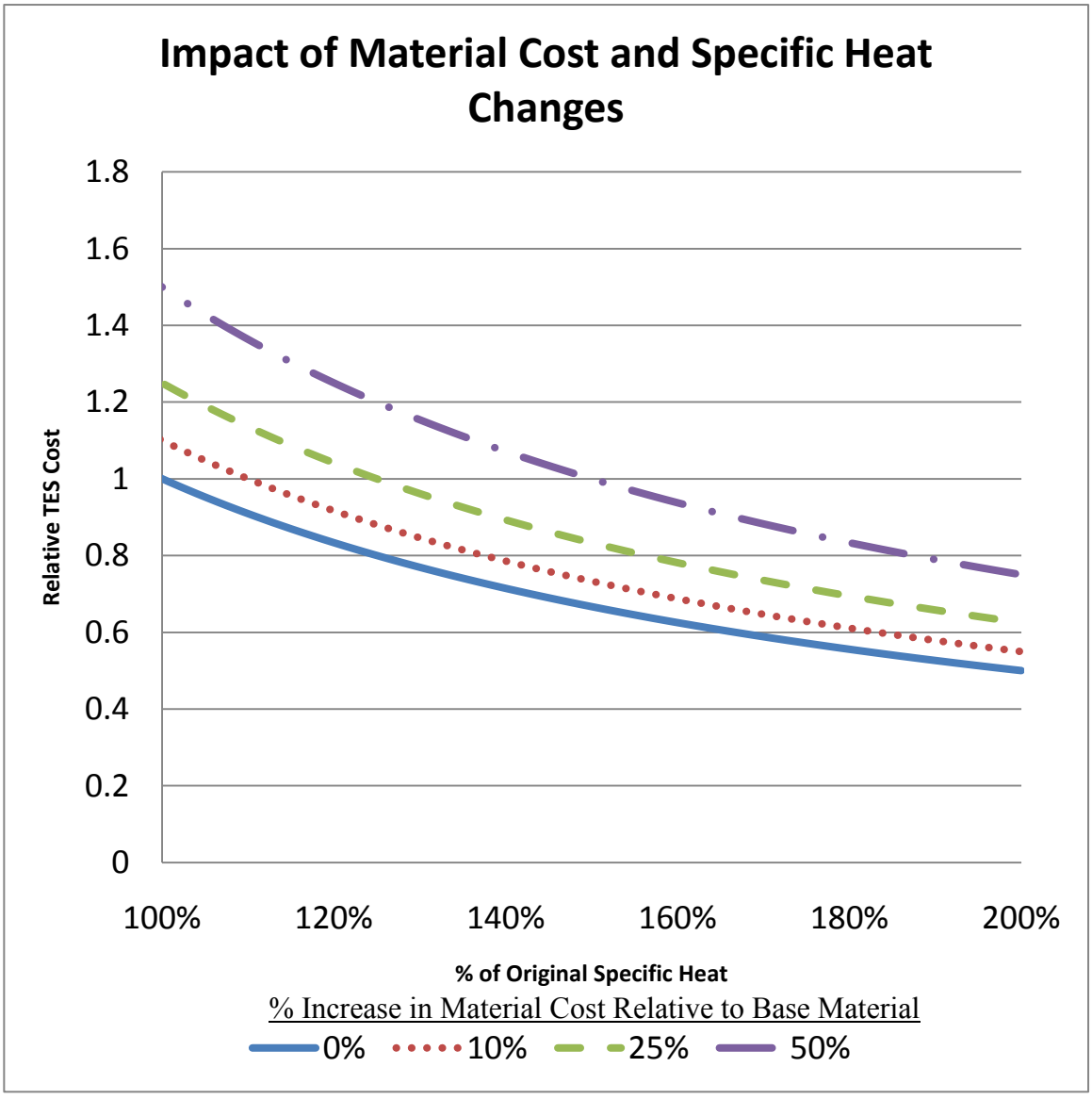

Fig. 7 Relative TES material costs due to the percent improvement in specific heat for a given percent increase in manufacturing costs.

Table 3
Predicted cost increase (%) for the created Hitec- Solar Salt and Al_2O_3 high temperature nanofluids.

Mass Fraction Al_2O_3	Increase in Material $/kg Cost	C_p Increase for 20% $/kWh$_t$ Reduction
0.1%	0.9%	126%
1.0%	8.8%	136%
10 %	87.6%	235%

In addition to lowering the TES material costs on a $/kWh$_t$ basis, improving the specific heat of the material results in secondary systems savings due to the need for smaller tanks, foundations, less insulation, etc.. The National Renewable Energy Laboratory has an Excel based CSPP modeling package known as Excelergy, which was used to estimate the total TES system costs. The model was modified to use the TES material specific heat capacity to determine the mass of TES material needed for a given system. The original version from NREL used the enthalpy of the TES material to perform this calculation. The methodology of the modified model is presented below:

1. Determine baseline thermal demand to operate the turbine at 100% capacity

$$ThermalInputDemand\ [MW_t] = \frac{TurbineOutput\ [MW_e]}{TurbineEfficency}$$

2. Determine the amount of energy to be stored by the TES

$$StoredEnergy[MWh_t] = ThermalInputDemand[MW_t] \times TESTime\ [hr]$$

3. Convert from energy storage units from MWh$_t$ to kJ

$$StoredEnergy\ [kJ] = StoredEnergy\ [MWh_t] \times \frac{1000\ kJ}{1\ \frac{MW-s}{MJ}} \times \frac{3600\ s}{1\ hour}$$

4. Determine mass of TES material needed for TES system

$$MassTESMaterial\ [kg] = \frac{StoredEnergy\ [kJ]}{AverageC_p\left[\frac{kJ}{kg-C}\right] \times \Delta T_{TES}[C]}$$

5. Determine tank volume

$$TankVolume\ [m^3] = \frac{MassTESMaterial\ [kg]}{DensityTESMaterial\ \left[\frac{kg}{m^3}\right]}$$

6. Use Excelergy model to determine tank costs

$$\xrightarrow{yields} TankCosts\ [\$]$$

7. Determine Material Costs

$$MaterialCosts[\$] = MassTESMaterial[kg] \times unitCosts\ \left[\frac{\$}{kg}\right]$$

8. Determine cost of TES system with 10% margin

$$TotalTEScost\ [\$] = (TankCosts\ [\$] + MaterialCosts\ [\$]) \times 1.1$$

9. Determine \$/kWh$_t$ cost of TES system

$$TEScost\ \left[\frac{\$}{kWh_t}\right] = \frac{TotalTEScost[\$]}{StoredEnergy[MWh_t]} \times \frac{1\ MWh_t}{1000\ kWh_t}$$

10. Determine \$/kWh$_e$ cost of TES system

$$TEScost\ \left[\frac{\$}{kWh_e}\right] = \frac{TotalTEScost[\$]}{TurbineOutput[MW_e] \times TESTime\ [hr]} \times \frac{1\ MWh_e}{1000\ kWh_e}$$

The cost inputs used in the Excelergy model appeared to be outdated as the cost of the nitrate eutectic was assumed to be 0.5 \$/kg whereas the price quoted by Coastal Chemical was 4.52 \$/kg. The potential cost discrepancies were accounted for by normalizing the predicted TES system costs by dividing the cost of the investigated systems by the predicted cost of the Andasol I type TES system. The results of this parametric study are presented in Fig. 8.

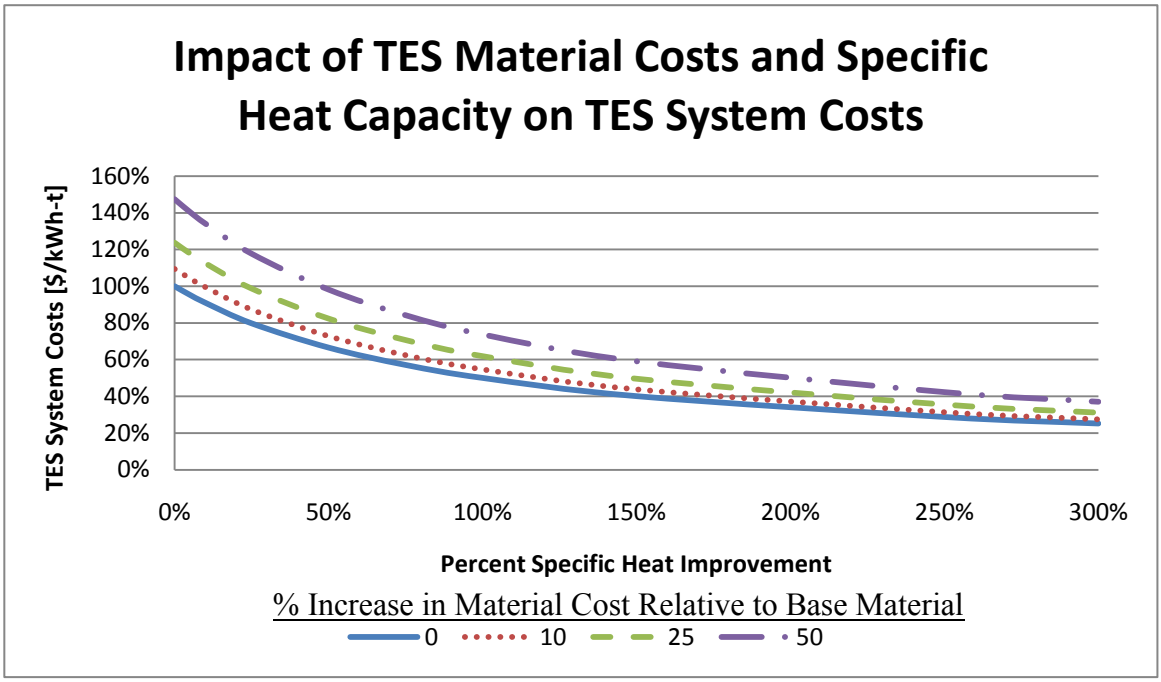

Fig. 8 Normalized TES costs predicted by NREL Excelergy model.

The family of curves in Fig. 8 represents TES system costs estimates for TES materials produced at 10, 25 and 50% cost increases. The 0% cost increase curve is provided for reference with the 0% specific heat improvement delineating the breakeven point for the other systems. The average specific heats of each of the created nanofluids were measured and used in conjunction with Fig. 8 to determine the cost effectiveness of the tested materials. In Section 3 the specific heats of the created nanofluids were also compared to the theoretical predictions of the models reported by Pak [13] and Zhou [11] to determine the ability of these models to predict the specific heat of high temperature nanofluids. The results of this comparison are given in Section 3.3. The experimental methods used to create and characterize the composite Solar Salt and alumina nanoparticle materials are presented in the following section, while the results are discussed in Section 3.

2. EXPERIMENTAL METHODS

2.1 Apparatus

The following instruments were used during the course of this investigation into the impact of introducing alumina nanoparticles into Hitec-Solar Salt. Mass balances, accurate to 10 μg, were used in the preparation of the composite materials to measure the mass of the constituent nanoparticle and Hitec-Solar Salt materials prior to the mixing process. An ultrasonic cleaner was used to sonicate the nanoparticles and Hitec-Solar Salt once they were placed into a solution. The composite material was recovered from the aqueous solution by drying it in a stainless steel pan which was heated by a hot plate. Finally, a differential scanning calorimeter (DSC) and laser flash analyzer (LFA) were used to determine the specific heat, thermal diffusivity, and thermal conductivity of the composite and base materials. Each of these instruments required the use of a mass balance to determine sample mass. Calipers were used to measure the sample disks prepared for the LFA, which required sample thickness and density measurements for determination of the thermal diffusivity and specific heat.

2.2 High Temperature Nanofluid Synthesis

The composites prepared for this research study were created using a three step aqueous mixing process which was adapted from the aqueous mixing process used by Pak and others to create water based nanofluids [13]. Introducing alumina nanoparticles into acidic solutions resulted in the development of a positive electrical charge on the surface of the suspended particles; this positive charge caused the nanoparticles to repel each other and results in well dispersed homogenous aqueous nanofluids [13].

To create the alumina-Hitec-Solar Salt composites at room temperature, a water solution with a pH of 3.2 was created using distilled water and a small amount of hydrochloric acid. The proper masses of Solar Salt and alumina nanoparticles were then measured into a 20 ml sample vial using a Sartorius CPA26P mass balance. After the desired mass fraction had been achieved, the vial was filled with the pH doped water solution to create approximately a 1%, by mass, aqueous solution of water, alumina nanoparticles, and Solar Salt. The target and actual masses for the desired base, 0.1, 1.0 and 10% by mass composite samples are given along with their associated volume fractions in Table 4 and Table 5 respectively. For consistency, each composite material will be referred to by its target mass fraction and constituent materials.

Table 4
Target mass fractions and constituent masses for the created composite materials.

Target Nanoparticle Fraction		Target Mass [mg]	
φ_m	φ_v	Al_2O_3	Hitec-Solar Salt
0.10%	**0.05%**	0.2	199.8
1%	**0.45%**	2	198
10%	**4.53%**	20	180

Table 5
Actual mass fractions and constituent masses for the created composite materials.

Actual Nanoparticle Fraction		Actual Mass [mg]	
φ_m	φ_v	Al_2O_3	Hitec-Solar Salt
0.12%	**0.05%**	0.368	315.58
1.14%	**0.52%**	2.31	199.89
9.67%	**4.38%**	20.138	188.184

To ensure that the samples were well mixed, the aqueous solutions were then sonicated for six hours using an ultrasonic cleaner. Precipitation of the alumina nanoparticles and/or the Solar

Salt was observed for the 1 and 10% composites. However, the precipitate appeared to go back into solution when the vials were agitated by hand.

Following sonication, the composite materials were dried by placing the solution into stainless steel pans which were heated by a hot plate. This drying method was used to maximize the heated surface area over which the material was dried to minimize drying time as a means of mitigating potential agglomeration and precipitation of the nanoparticles.

The specific heat of the composites was measured using a differential scanning calorimeter. The instrument and measurement technique are described in Section 2.3, while the results of the composite material characterization are presented in Section 3.

2.3 Material Characterization-Instrumentation and Technique

A differential scanning calorimeter was used to determine the specific heat of the composite materials. To determine the uncertainty and suitability of the instrument, the DSC was characterized using a set of specific heat standards provided by Netzsch Instruments. Additionally, specific heat measurements of the solid phase base material were made on the DSC and confirmed on an LFA to build confidence in the measurement technique used. The operating principles and characterization of the DSC and LFA are presented in the following sections in greater detail.

2.3.1 Differential Scanning Calorimeter

The primary instrument used for this research was the STA 409 PC Luxx by Netzsch Instruments. This instrument has a DSC/TG probe which was used to determine the specific heat of the base solar salt and the composite materials. The Netzsch instrument consists of a tube furnace, balance, and DSC/TG probe. The probe has two pan locations to hold the sample

and reference crucibles. Platinum power wires and thermocouples are attached to the underside of the two pan locations. The power wires are used to supply power to the two pan locations to maintain the crucibles at equal temperatures as measured by the thermocouples. The differential power required to maintain the sample and reference crucibles at the same temperature is recorded as the DSC signal.

The instrument assumes that the probe is perfectly centered within the tube furnace and that the reference and sample crucibles, which are assumed to be identical to each other, are subject to symmetric heat fluxes. In reality, the assumptions of perfectly symmetric heat flux and perfectly identical crucibles are unobtainable. These inconsistencies are captured in a baseline or "correction" runs. The correction run is used to determine the differential power signal due to asymmetric heat fluxes, differences in the sample and reference crucible, as well as the mass changes due to buoyancy effects as the purge gases are heated as the instrument runs through the programmed temperature profile.

The general procedure for performing a specific heat measurement using the STA 409 consists of performing a baseline or correction measurement, a sapphire standard measurement, and finally a sample measurement. This procedure is described in great detail in ASTM E 1269, the standard for the determination of specific heat by using a DSC [14]. Each measurement profile - baseline, standard, and sample - is identical and consists of two isothermal segments and a dynamic heating segment. The isothermal segments occur at the beginning and end of the measurement at the lower and upper temperature limits. These isothermal segments are meant to ensure that the baseline, standard, and sample runs have the same initial and end conditions. The ASTM E 1269 specifies the use of a 20 °C/min heat rate during the dynamic heat segment of these measurements [14]. The standard states that different heat rates can be used for the

dynamic heating segment of the specific heat measurements, but that any deviation from the 20 °C/min heating rate needs to be reported along with any subsequently published results.

The Netzsch Instruments user's manual suggests that heating rates between 10 and 20 °C/min be used when performing a specific heat measurement [15]. The effect of the heating rate on the accuracy and precision of the measured specific heat values were investigated to determine the optimum heat rate for subsequent specific heat measurements of the composite and base materials. For this experiment, the 6 mm diameter, 0.75 mm thick sapphire standard provided by Netzsch Instruments was utilized as both the standard and "unknown" sample measurements. The same standard was used to maintain the dynamic heating rate of the specific heat measurements as the sole variable during the course of this part of the instrument characterization.

The heat rates investigated during this experiment were 10, 15, and 20 °C/min. The specific heat was measured using the ASTM E 1269 method which requires two empty crucible pans with lids to be placed into the instrument to establish a baseline for the future sapphire standard and unknown sample measurements. The baseline, sapphire and sample measurements were carried out using the same heating profiles [14] for each of the heating rates of interest.

For each of the heating rates, the measurement was started at an initial temperature of 220 °C. The instrument was then heated at 10 °C/min to 250 °C. The crucibles were then held at 250 °C for 10 minutes to allow the instrument to equilibrate at the starting temperature. The instrument was then heated to 450 °C using the dynamic heating rate under investigation. A final 10 minute isotherm at 450 °C was used to ensure the crucibles equilibrated at the upper temperature of interest. The 250 to 450 °C temperature range was selected because it was to be used to measure the specific heat of the composite and base materials in this range, which brackets the 280 °C to 395 °C operating range of most parabolic trough concentrating solar

power plants. Additionally, this thermal profile avoids the nitrate melting and decomposition temperatures. The heating profile for the 10 °C/min heat rate is shown in Fig. 9 as a reference.

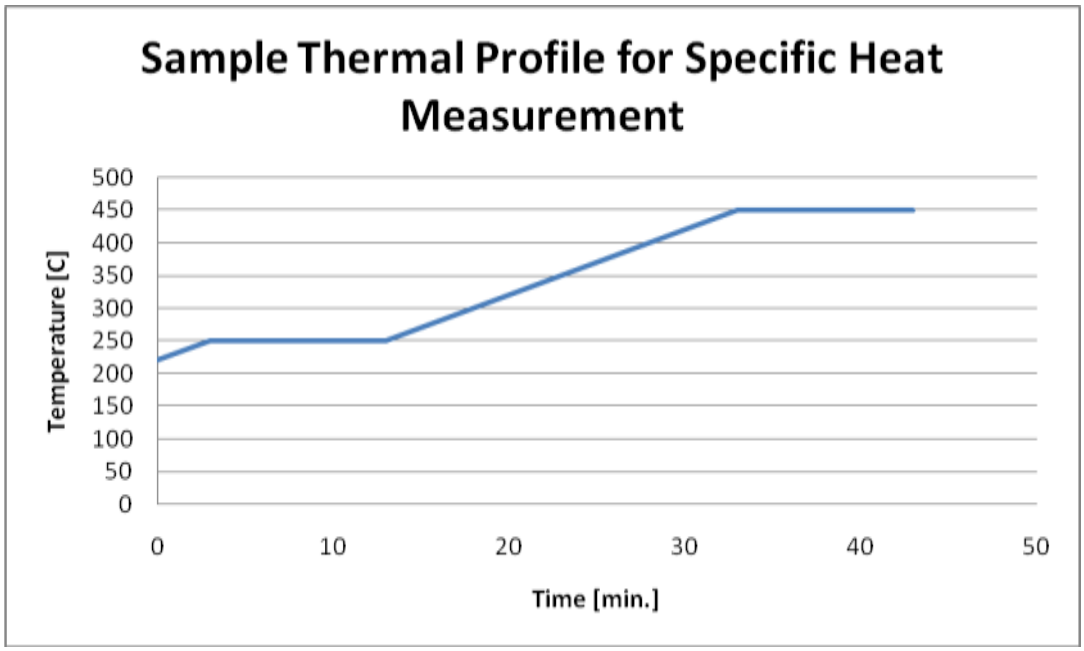

Fig. 9 Thermal profile used for the 10 °C/min measurement of the sapphire standard.

Netzsch provides a specific heat software package which was used to calculate the specific heat of the sapphire standard. Two different algorithms are provided; the ratio and ASTM methods solve the same basic Eq. 4 [15]. The ASTM method has an additional algorithm which corrects for temporal drift from in the machine by applying a linear correction to the DSC signals for the sapphire and sample measurement. The formula for this correction is given in Eq. 5 [15].

Determination of the specific heat of an unknown sample using a DSC and a standard with a known specific heat

$$C_{p,sample} = \frac{m_{standard}}{m_{sample}} \times \frac{DSC_{sample} - DSC_{baseline}}{DSC_{standard} - DSC_{baseline}} \times C_{p,standard} \quad (4)$$

Netzsch's ASTM specific heat algorithm for DSC signal correction

$$DSC_{ASTM}(t) = DSC(t_1) + \frac{DSC(t_2) - DSC(t_1)}{t_2 - t_1} \times (t - t_1) \quad (5)$$

For the purposes of this investigation, both the ratio and ASTM algorithms were used to calculate the specific heat of the sapphire standard so that the impact of using these two different methods could be characterized and discussed. Both methods showed relatively good agreement with the provided Netzsch standard literature values. The results and percent error for the different heat rates and evaluation algorithms are provided in Fig. 10 - Fig. 13.

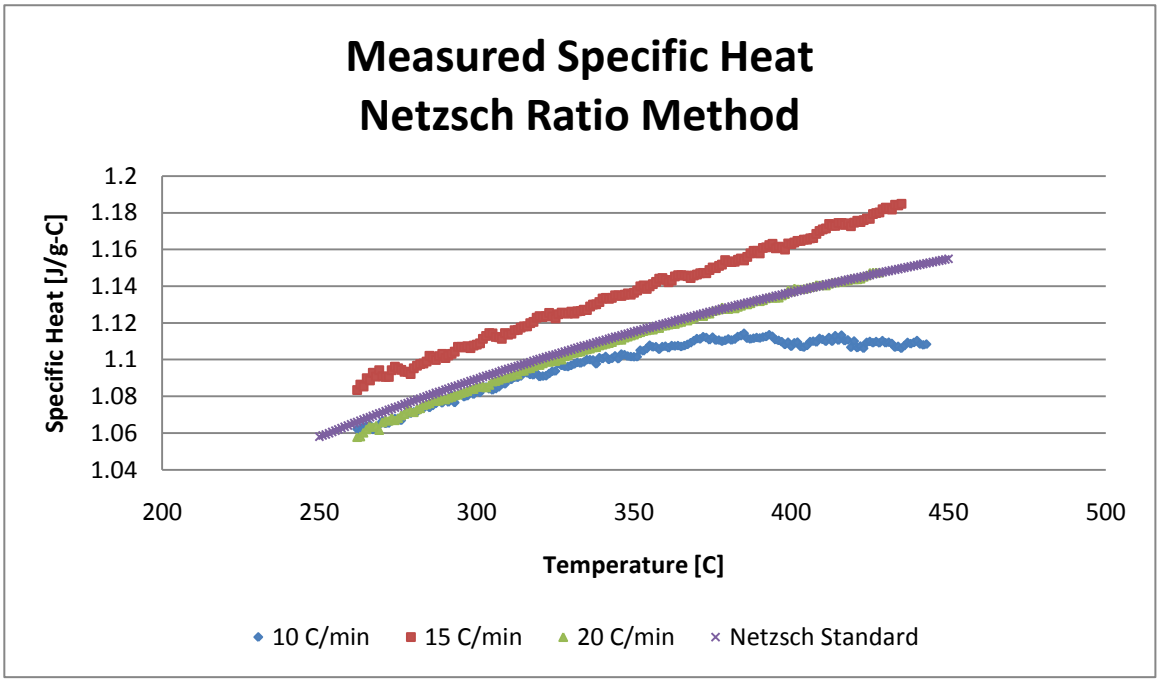

Fig. 10 Specific heat values calculated for the sapphire standard using the Netzsch Ratio algorithm for the tested dynamic heating rates.

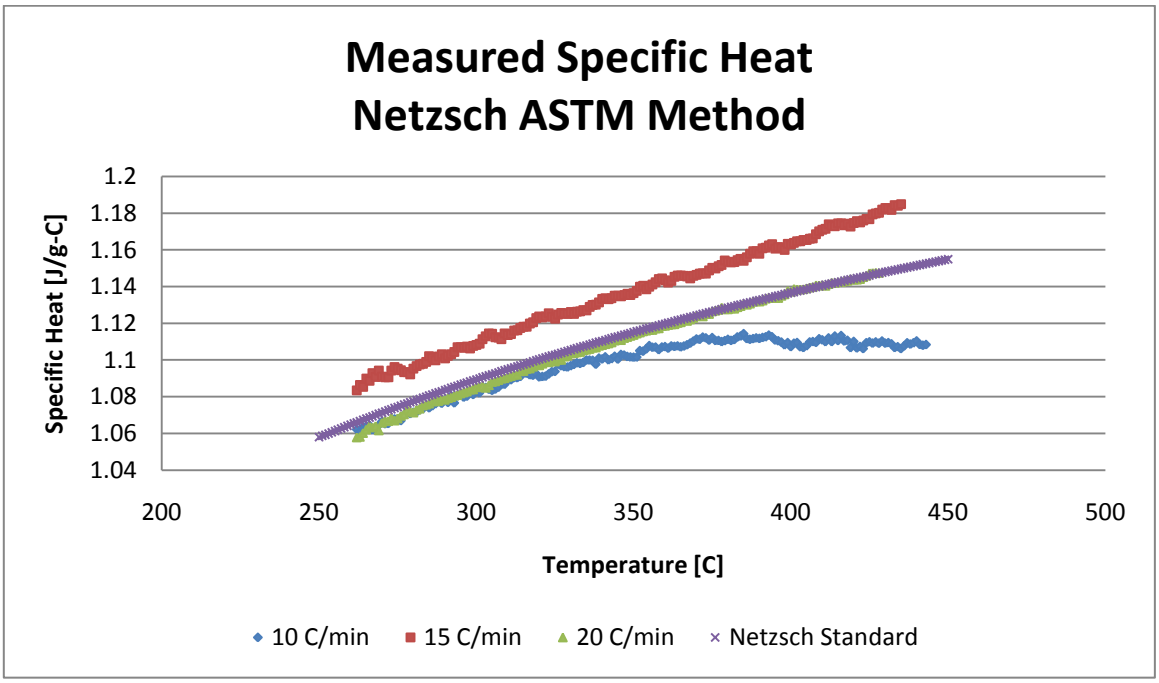

Fig. 11 Specific heat values calculated for the sapphire standard using the Netzsch ASTM algorithm for the tested dynamic heating rates.

The percent error for the measured specific heat of the sapphire standard was calculated using Eq. 6.

Percent error of the calculated specific heat

$$\% \, Error = \frac{C_{p,Calculated} - C_{p,Literature}}{C_{p,Literature}} \tag{6}$$

For each of the heat rates, the absolute percent error was less than 4% over the temperature range of interest. The 20 °C/min heat rate had the highest accuracy or the lowest percent error of each of the tested heat rates.

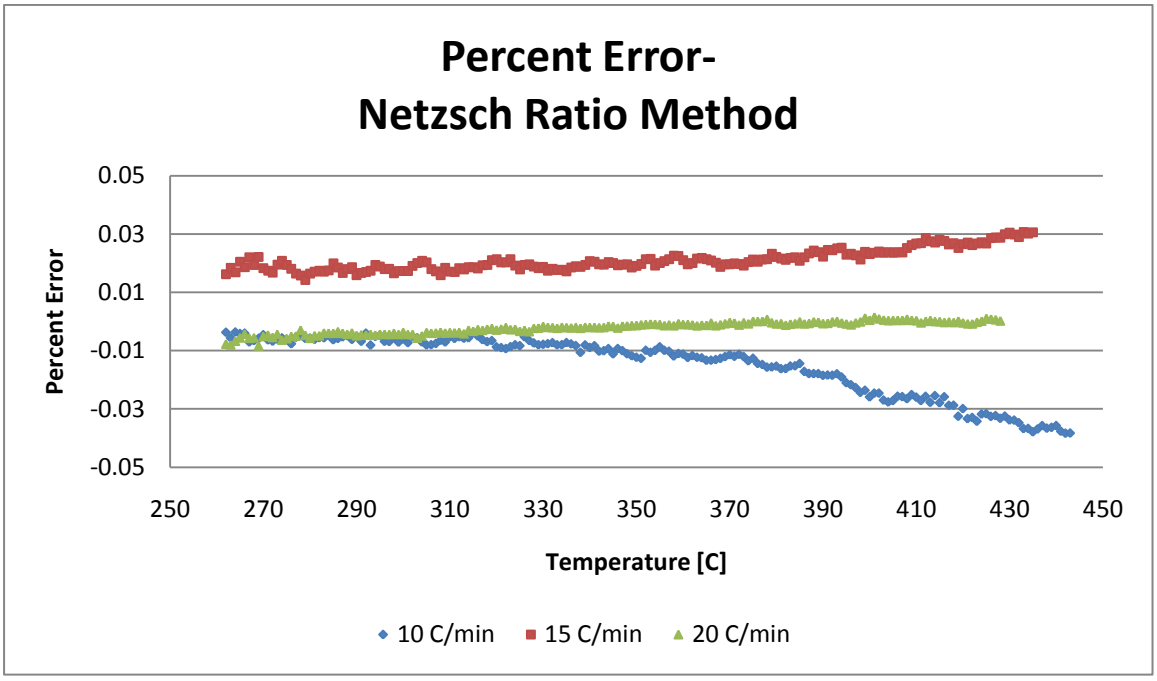

Fig. 12 Percent error for the specific heat of the sapphire standard calculated using the Netzsch ratio algorithm.

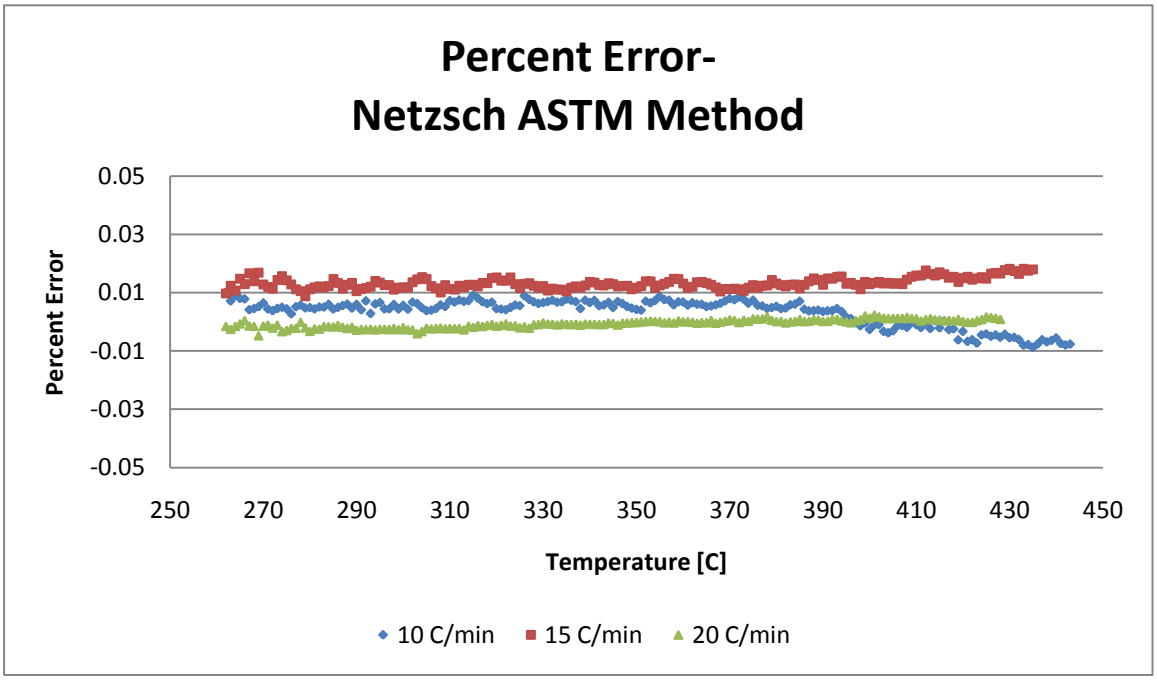

Fig. 13 Percent error for the specific heat of the sapphire standard calculated using the Netzsch ASTM algorithm.

Fig. 14 shows the impact of the heat rate on the spread of the data as well as the average error in the calculated specific heat. The figure shows that higher heat rates result in more precise data sets which have less spread over the temperature range of interest. Accuracy appears to be optimized at the 20 °C/min heat rate as well, but there does not appear to be a clear correlation between the heat rate and the minimum, maximum, or average errors.

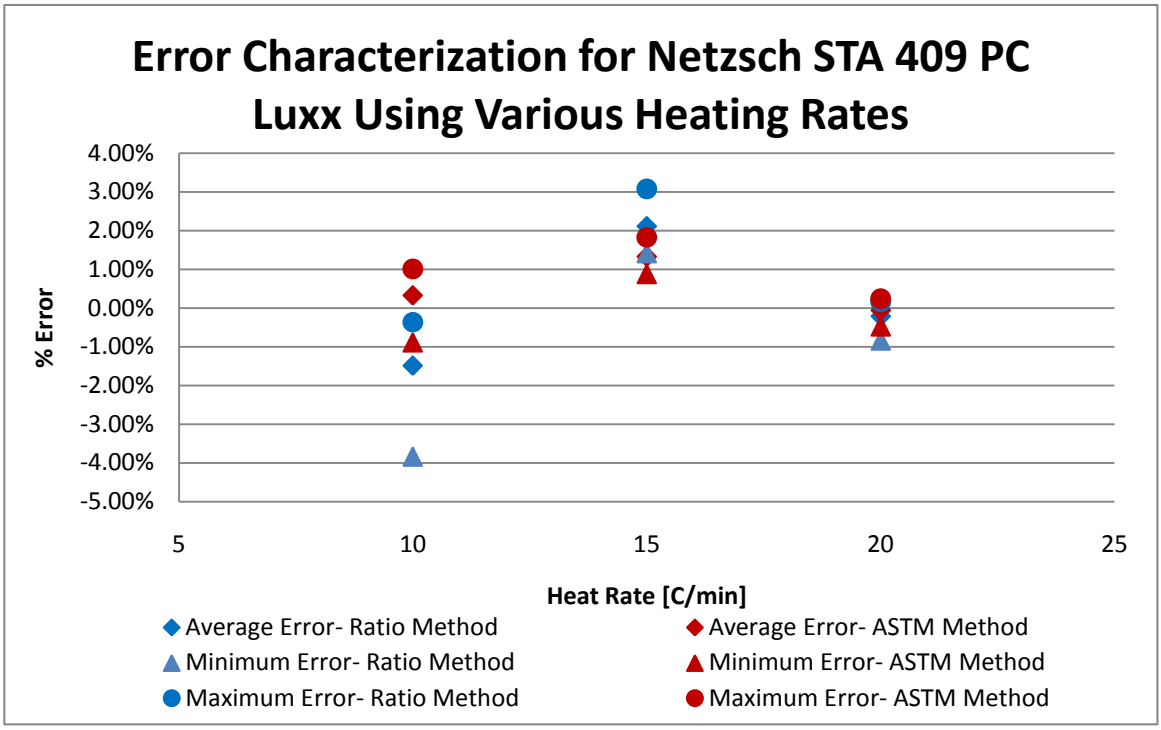

Fig. 14 Error statistics for the specific heat measurement of a sapphire standard using the Netzsch STA 409.

Despite the increased accuracy and precision observed when the 20 °C/min heat rate was used for the specific heat measurement, the higher heat rate has some drawbacks. Fig. 15 shows that as the heat rate is increased, more data in the area of interest is "lost" or cannot be determined by the Netzsch software. For each heating rate, the first 12 data points could not be determined and an additional 7, 15, and 22 data points were lost at the upper temperature range

for the 10, 15 and 20 °C/min heat rates respectively. The loss of this data was due to the transient heating of the sample at the upper and lower temperature bounds due to the thermal lag and thermal inertia of the sample respectively. Identifying this data loss was beneficial to the sample measurements because it confirms the temperature range is sufficient to ensure data is collected throughout the Andasol 1 temperature range of interest.

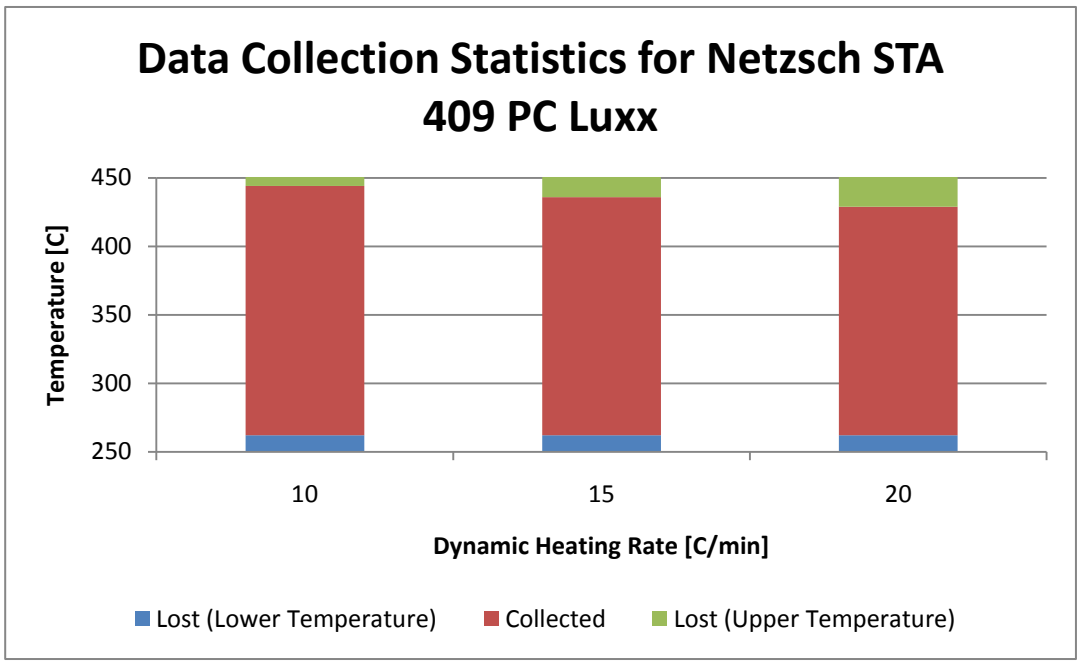

Fig. 15 Data collection statistics for the investigated dynamic heating rates.

It appears the ASTM method delivers slightly more accurate data then the ratio method; however, it is important to note that the determination of the parameters t_1 and t_2 in Eq. 6 are subject to the determination of the instrument user, whereas the ratio method will always yield consistent specific heat values for an individual measurement regardless of the analyst. In general, the ASTM method seems to work best when the times t_1 and t_2 are selected such that the DSC signals at these times are at or near zero. This may not always be possible as signal

degradation has been observed in previous measurements carried out on the salt and salt-nanoparticle composites. During the course of testing, both methods were utilized to determine the specific heat of the material of interests with deference given to the ASTM method unless signal degradation made the proper selection of t_1 and t_2 impossible. In these cases, the ratio method was utilized because its algorithm for the calculation of specific heat does not rely on the isothermal DSC signals for the determination of the sample specific heat.

In addition to characterizing the interaction of the measurement heat rate and measurement accuracy and precision, the impact of the difference between the sample and standard masses was also investigated. The impetus for this investigation was an article written in 1972 by Vuclelic [16] which discussed the impact of sample mass on the specific heat measured by a DSC. In the work, Vuclelic showed that as the sample mass increased beyond 30 mg, the resulting change in the DSC signal amplitude decreased resulting in an increased percent error when compared to the measured specific heat in the region of proportional amplitude response [16]. This phenomenon was not observed in the data collected on the STA 409. As seen in Fig. 16, the STA 409 DSC signal amplitude is proportional to the sample mass well beyond the 30 mg reported by Vuclelic.

The data collected to verify that the STA 409 DSC signal was proportional to sample mass was used to investigate the impact of the difference between the standard and sample masses; a description of the standards and their masses is provided in Table 6. The 84 mg standard, Standard 2, was used in the second or standard run for each of the specific heat measurements. A summary of the specific heat runs is given in Table 7.

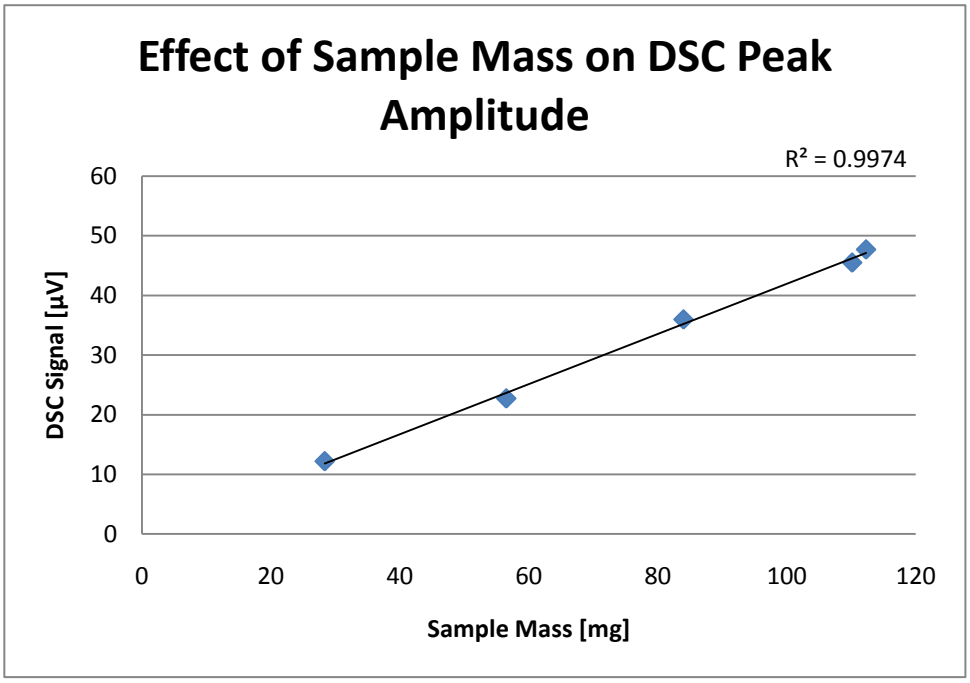

Fig. 16 Correlation between DSC signal and sample mass.

Table 6
Netzsch provided specific heat standards used in the determination of the impact of differences in standard and sample mass on the accuracy of specific heat measurements.

Standard #	Crystalline Structure	Mass [mg]
Standard 1	Monocrystalline Al_2O_3 (Sapphire)	28.325
Standard 2	Monocrystalline Al_2O_3 (Sapphire)	83.967
Standard 3	Monocrystalline Al_2O_3 (Sapphire)	112.283
Standard 4	Polycrystalline Al_2O_3 (Alumina)	56.483
Standard 5	Polycrystalline Al_2O_3 (Alumina)	110.133

Table 7
Description of the runs used to characterize the impact of the difference between standard mass and sample mass (Δm) on the accuracy of specific heat measurements.

Measurement #	Standard Run	Sample Run	Δm [mg]
Measurement 1	Standard 2	Standard 1	55.64
Measurement 2	Standard 2	Standard 2	0.00
Measurement 3	Standard 2	Standard 3	-28.32
Measurement 4	Standard 2	Standard 4	27.48
Measurement 5	Standard 2	Standard 5	-26.17

To expand the data set, the specific heat of Standard 2 was determined by using the standard from the sample run. This technique differs from that prescribed in ASTM E 1269, but the resulting specific heat measurements appeared to be highly accurate, within ± 2% error as shown in Fig. 17 for Measurement 2 in Table 7.

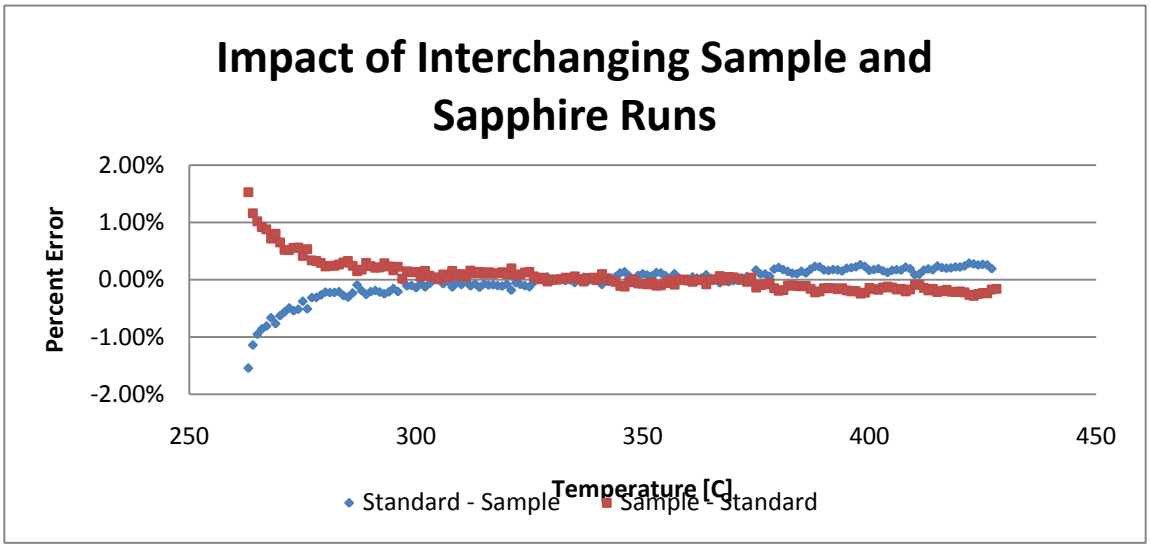

Fig. 17 Percent error for the measured specific heat for Measurement 2 of the data set used to characterize the impact of standard and sample mass differences.

The minimum, maximum, and average percent error for each of the specific heat measurements were determined to quantify the impact of differences in the standard and sample masses. The specific heat for this data set was calculated using both the ratio and ASTM algorithms; the results of these calculations are given in Fig. 18 and Fig. 19 respectively.

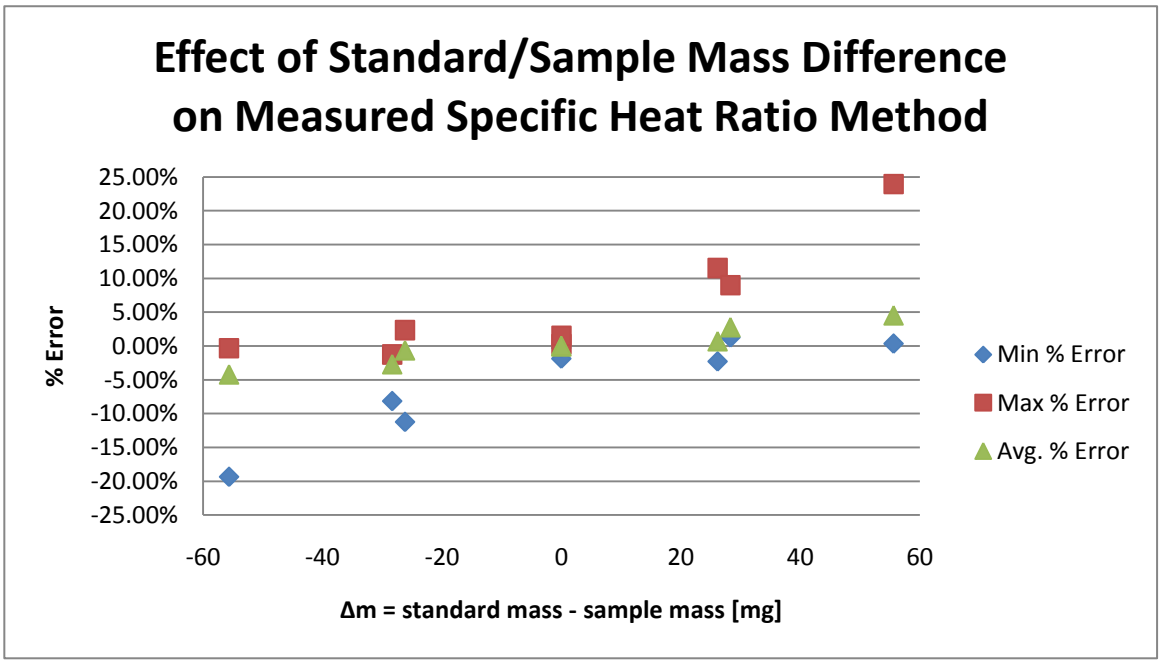

Fig. 18 Impact of standard /sample mass differences on the percent error of the specific heat measurement of Netzsch provided C_p standards determined using the ratio algorithm.

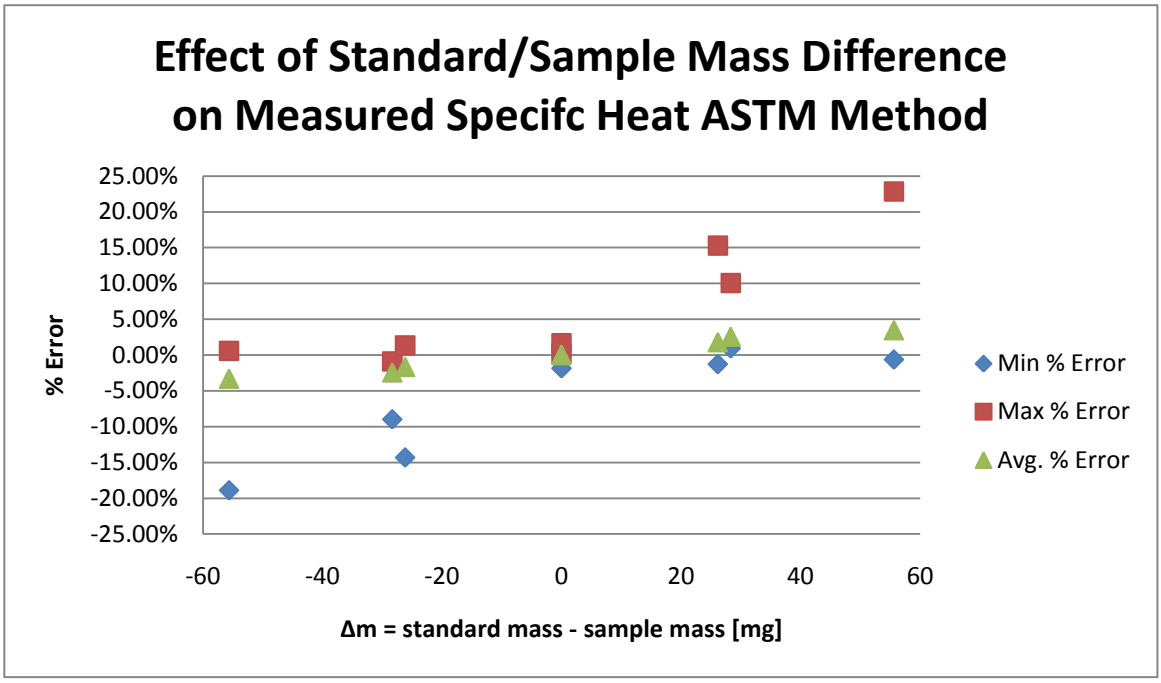

Fig. 19 Impact of standard /sample mass differences on the percent error of the specific heat measurement of Netzsch provided C_p standards determined using the ASTM algorithm.

Finally, the percent error for the average specific heat over the 250 - 450 °C temperature range was calculated. The average specific heat over the temperature range of interest has been used as the foundation of TES material costs in various journal articles and reports which discuss the costs of thermal energy storage systems. In general, the material costs are approximated on a $/kWh$_t$ basis using (7). The percent error between the calculated average specific heat and the literature average specific heat over the temperature range of interests are plotted for the tested standard and mass differences in Fig. 20.

Figure of merit for DOE thermal energy storage media on a [$/kWh$_t$]

$$MediaCosts\left[\frac{\$}{kWh_t}\right] = \frac{MaterialCosts\left[\frac{\$}{kg}\right]}{AverageC_p\left[\frac{kJ}{kgK}\right] \times \Delta T[K] \times 2.778E-4\left[\frac{kWh_t}{kJ}\right]} \quad (7)$$

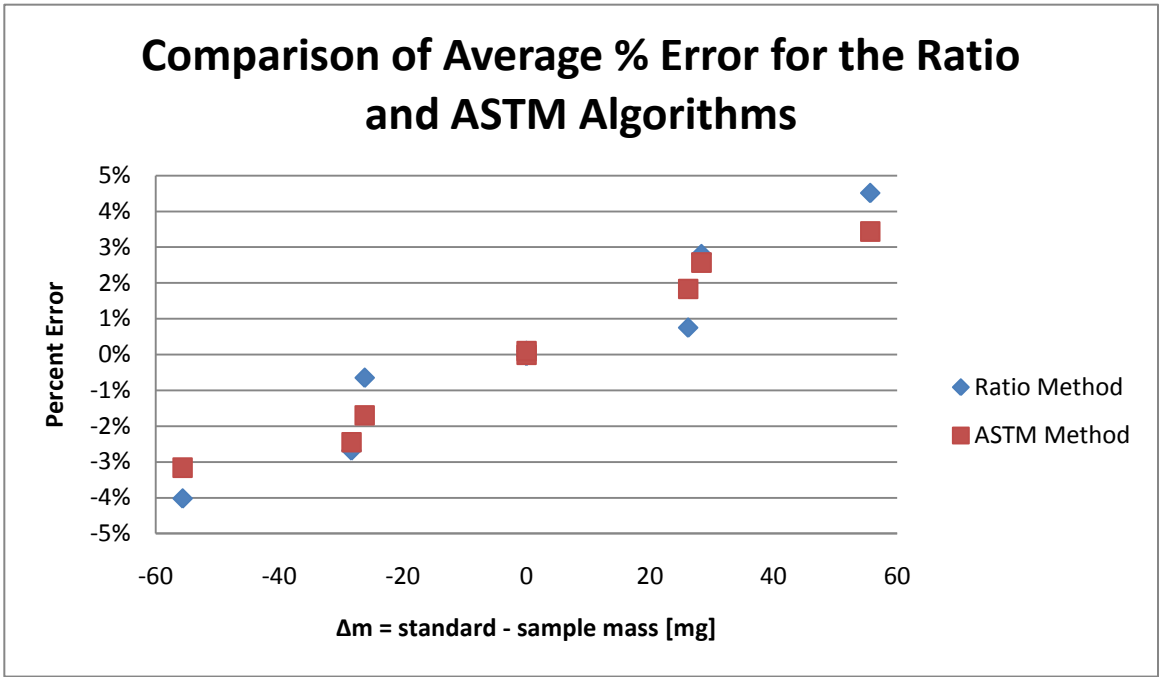

Fig. 20 Correlation between percent error of the measured specific heat and the difference between standard and sapphire masses for the two provided Netzsch algorithms.

After characterizing the STA 409's ability to accurately measure the specific heat of the Netzsch C_p standards, the following procedures were adapted: Prior to each set of measurement runs, the sample and reference crucibles and their respective lids were cleaned using an ultrasonic cleaner and a sulfuric acid bath. The crucibles were then rinsed in ethanol and dried. The masses of both crucibles were measured and recorded using a Metler Toledo AL204 mass balance capable of measuring samples to within 0.1 mg. The sample and reference crucibles were then placed into their respective locations on the DSC/TG sample probe. Each measurement set consisted of three runs each: a baseline run with just the empty crucibles, a standard run with the 28 mg sapphire standard in the sample crucible, and a sample run in which the material of interest was placed into the sample crucible. The results of these specific heat measurements are presented in Section 3.

2.3.2 Light Flash Analyzer

To confirm the specific heat values measured by the DSC, a light flash analyzer was used to calculate the specific heat of Hitec-Solar Salt in the solid phase. As in the case of the DSC, the LFA was characterized by performing a set of thermal diffusivity measurements using a set of standards provided by Netzsch Instruments. The LFA 447 used during the course of this research has an operating range of 20-300 °C. The device uses a Xenon bulb to produce the light flash used to heat the samples to be measured.

An LFA is traditionally used to determine the thermal diffusivity by solving the transient 1-D heat equation. ASTM E 1461, *Standard Test Method for Thermal Diffusivity by the Flash Method* [17] describes the theory and procedure for determining the thermal diffusivity and specific heat using this type of instrument. As described in ASTM E 1461 the 1-D Heat Eq. 8, is solved under the assumptions that the samples are homogenous, isotropic, and that there is minimal heat loss from the sample surfaces.

1-D Heat Eq.

$$\frac{\partial T}{\partial t} = \alpha \frac{\partial^2 T}{\partial x^2} \tag{8}$$

As in the case of the DSC, the initial assumptions made for the determination of thermal diffusivity are seldom fully realized. As a result, several different models have been proposed and published for the determination of thermal diffusivity. Many of which are included in Netzsch's thermal analysis software which accompanies the LFA 447 [18]. For the purposes of the characterization runs performed using the Netzsch standards, the Netzsch radiation plus pulse correction algorithm was used in the determination of the standards' thermal diffusivity. This

model calculated the thermal diffusivity to within ± 5%, which is within the range specified by the manufacturer. Following these characterization runs, the LFA was used to verify the solid phase specific heat measured by the DSC; due to the limited temperature range of the device, the LFA was not used for the characterization of any other materials.

3. RESULTS AND FINDINGS

3.1 Base Material Characterization

3.1.1 Solid Phase Characterization

To increase confidence in the DSC measurement technique, three samples of Hitec-Solar Salt were measured in the DSC and the calculated specific heat values were compared to three different Solar Salt samples measured in the LFA 447. The LFA determines specific heat using Eq. 9 [18]. The average specific heat values measured by the DSC and LFA are presented in Fig. 21 along with the average solid phase specific heat provided by the manufacturer, Coastal Chemical.

Determination of specific heat using the flash method

$$C_p^{Sample} = \frac{T_\infty^{Ref.}}{T_\infty^{Sample}} \times \frac{Q^{Sample}}{Q^{Ref.}} \times \frac{V^{Sample}}{V^{Ref.}} \times \frac{\rho^{Ref.} D^{Ref.}}{\rho^{Sample} D^{Sample}} \times \frac{d_{Orifice}^{2,Sample}}{d_{Orifice}^{2,Ref.}} \times C_p \quad (9)$$

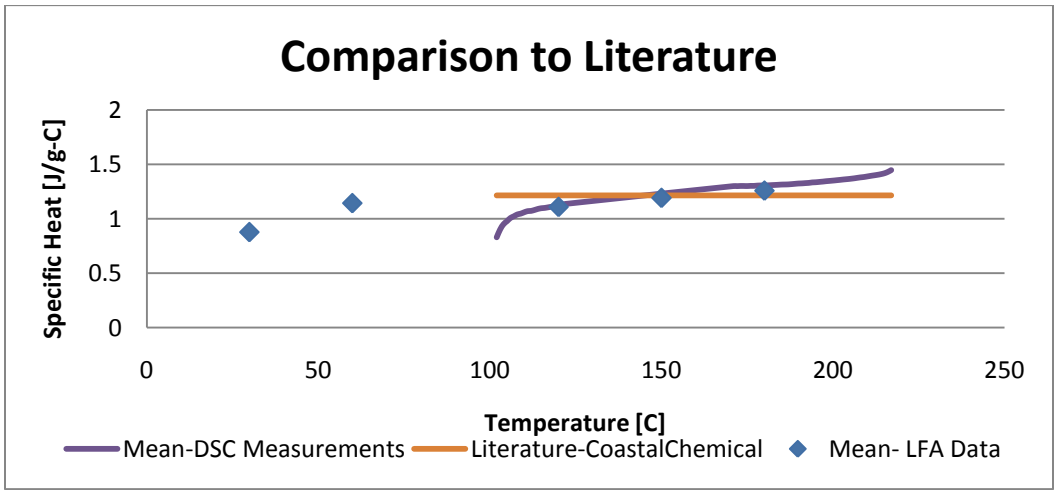

Fig. 21 Specific heat values determined for solid phase Hitec-Solar Salt using a STA 409 and a LFA 447.

Measurement of the solid phase Solar Salt in the DSC revealed the presence of a contaminant which melted at around 130 ˚C. It is possible that this contaminant is a binding agent or plastic used in the manufacturing and/or packaging of Hitec-Solar Salt. The source of this contamination was not pursued vigorously because it occurred in a temperature range which was not pertinent to the main objectives of this research. Instead, the data taken over the temperature ranges at which the melt occurred were removed. As shown in Fig. 21, the specific heat values calculated by the DSC and LFA overlay each other quite well. Additionally, the average of these measured values also agrees to within ±3% with the literature value provided by Coastal Chemical [19].

3.1.2 Liquid Phase Characterization

To evaluate the potential for enhancing the specific heat of Hitec-Solar Salt via the introduction of nanoparticles, the specific heat of the base material was characterized for comparison to the composite materials which were created and characterized during the course of this research. The measurement began at an initial temperature of 230 ˚C. The sample was then heated at 10 ˚C/min to 250 ˚C; a 10 minute isotherm at 250 ˚C was used to ensure the sample equilibrated at 250 ˚C prior to the dynamic heating segment over which the specific heat of the material was meant to be measured. Following the initial isotherm, the sample was heated at 20 ˚C/min to 450 ˚C. A final isotherm at 450 ˚C was used to ensure the sample reached the upper temperature of interest. This temperature range was selected to ensure that specific heat data could be collected in the 292-386 ˚C operational temperature range of the Andasol 1 parabolic trough concentrating solar power plant (CSPP) in Spain which currently utilizes a 60-40 sodium and potassium nitrate eutectic similar to Hitec-Solar Salt in the plant's two tank thermal energy storage (TES) system.

Three different samples were measured using the procedure outlined in ASTM E 1269 which calls for baseline, standard and sample measurements to be performed over identical thermal profiles [14]. To follow the Netzsch recommended procedures, the samples where only measured one time [15]. The same platinum crucible and lid was used for each of the sample measurements. Following each measurement, the sample crucible and lid were cleaned in sulfuric acid bath and rinsed in ethanol.

The resulting data was analyzed using Netzsch's ratio method in their provided specific heat software package. The ratio method, which was shown to be slightly less accurate than the available ASTM method, was utilized due to the signal degradation, shown in Fig. 22, during the final isotherm. The reason for this degradation shown is unknown. The resulting specific heat measurements are plotted in Fig. 23. The average specific heat of this measurement set and the accompanying confidence intervals are plotted along with three available references in Fig. 24. The reported Coastal Chemical value is the average liquid phase specific heat reported by the manufacturer of Hitec-Solar Salt [19]. The reported SAM Model values were calculated using the linear equation which is used to calculate the specific heat of nitrate eutectics in the Solar Advisor Model software package created by the Department of Energy (DOE). The referenced NREL value is the average specific heat for nitrate eutectics reported in *Survey of Thermal Energy Storage Systems for Parabolic Trough Power Plants* for the National Renewable Energy Laboratory in Colorado [6]. Finally, the percent errors with respect to the reference values are presented in Table 8.

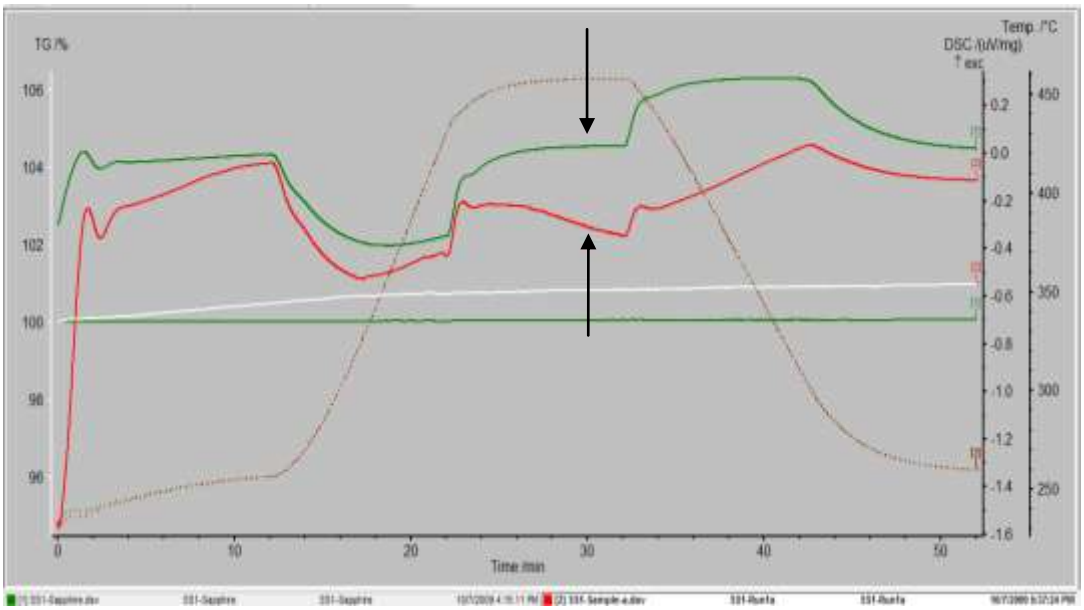

Fig. 22 Netzsch STA 409 DSC output showing the sample's signal degradation (red).

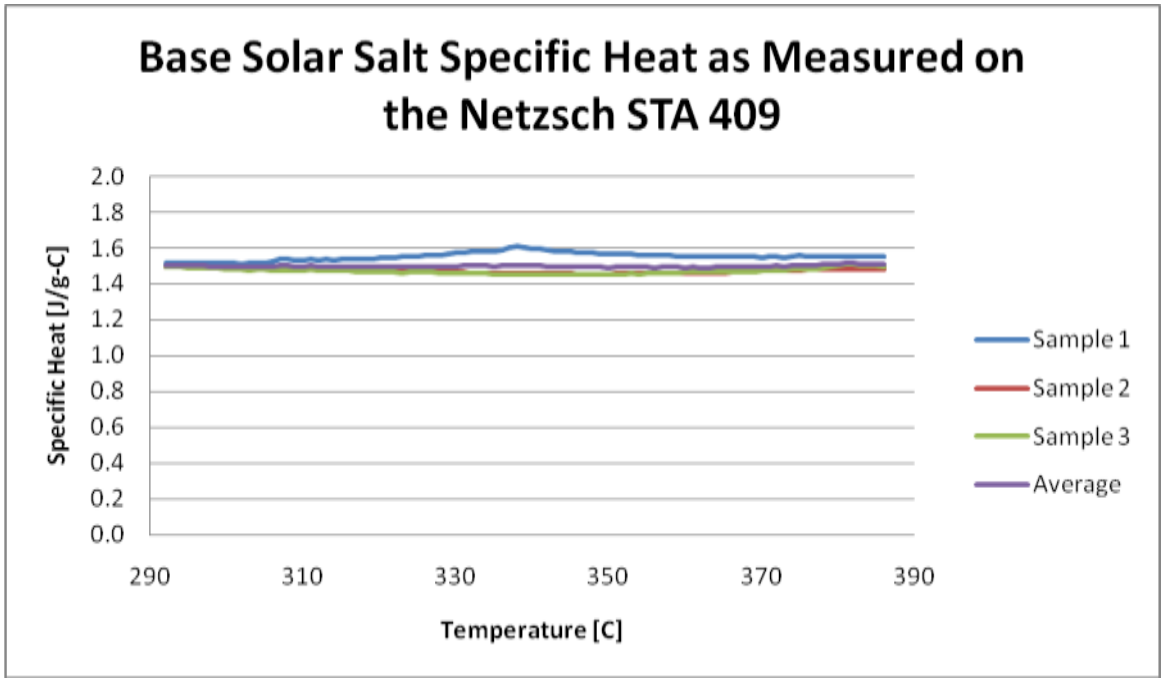

Fig. 23 Measured specific heat values for each of the three sample runs as well as their average for the 292-386 °C operating range of Spain's Andasol 1.

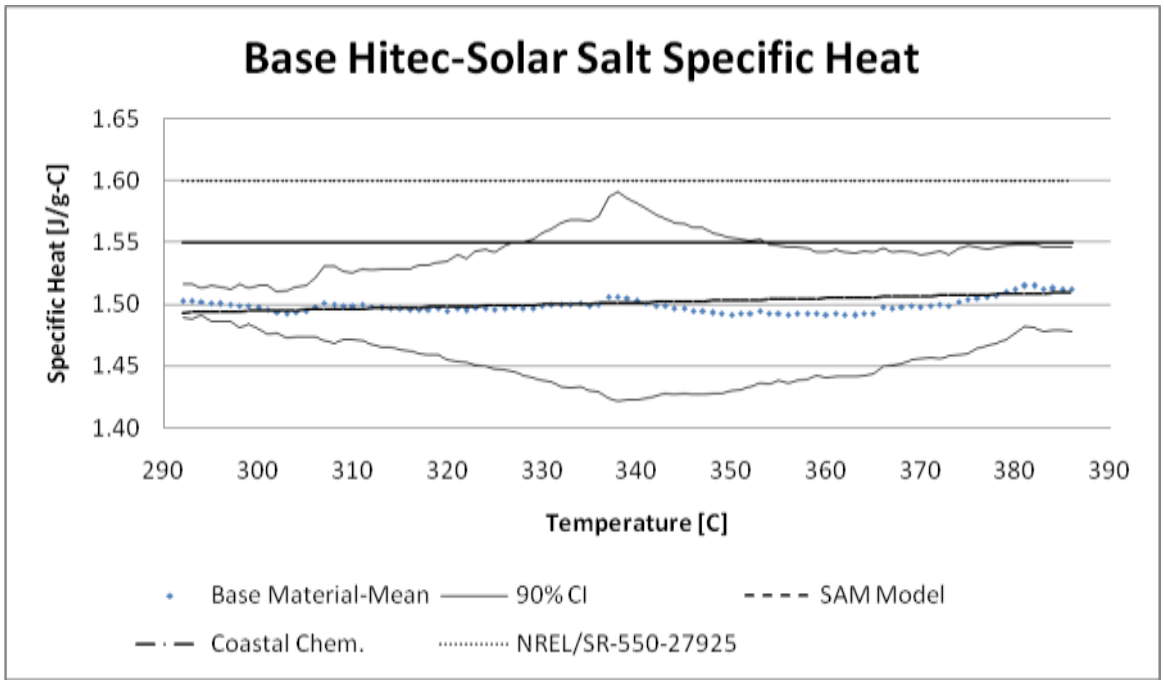

Fig. 24 Measured Hitec-Solar Salt and available reference specific heat values.

Table 8
Calculated percent error for each of the specific heat sample measurements with respect to the three available literature values**.**

Sample Number	Coastal Chem.	SAM Model	NREL/SR-550-27925
1	0.18%	3.43%	-2.95%
2	-5.00%	-1.91%	-7.97%
3	-5.13%	-2.05%	-8.09%
Average (Absolute)	3.44%	2.46%	6.34%

The measured average specific heat for Hitec-Solar Salt shows excellent agreement, less than 3.5% error, with the reference value provided by the SAM model specific heat equation for the nitrate eutectic. The measured value also agrees to within ±5% with the Coastal Chemical specific heat values. The NREL reference specific heat value was only given to two significant digits, 1.6 J/g-˚C [6], which may have been rounded off from the 1.55 J/g-˚C reported by Coastal

Chemical [19]. The relatively good agreement with the available literature provided the necessary confidence in the experimental method to justify proceeding with the characterization of the composite materials. The results of the high temperature nanofluid specific heat measurements are available in Appendix A. A discussion of these results is presented in the following section.

3.2 Discussion of Results

The majority of the results discussed in this section are derived from the specific heat measurements taken over the 292-386 ˚C operating temperature range of the Andasol 1 thermal energy storage system in Spain. Specific heat data was taken over a broader temperature range to ensure that any potential data loss occurred outside of the 292-386 ˚C range of interest. Analysis of this larger temperature range 262-428 ˚C reveals an anomaly in the specific heat data collected during the characterization of the 1% Solar Salt-Alumina nanofluid. This data is outside of the scope of this research because it occurs outside the range of operating thermal energy storage systems. However, it will be discussed at the close of this section.

The measured mean specific heats for each of the Solar Salt and alumina high temperature nanofluids are plotted in Fig. 25. The percent change in specific heat for each of the nanofluids with respect to the base fluid is shown in Fig. 26. A linear regression analysis reveals a strong positive correlation between the Andasol 1 average specific heat of the high temperature nanofluids and the concentration of alumina nanoparticles Fig. 27. This “Andasol 1 average specific heat” is the average of the measured specific heats taken over the 292-386 ˚C operating range of Andasol 1’s thermal energy storage system.

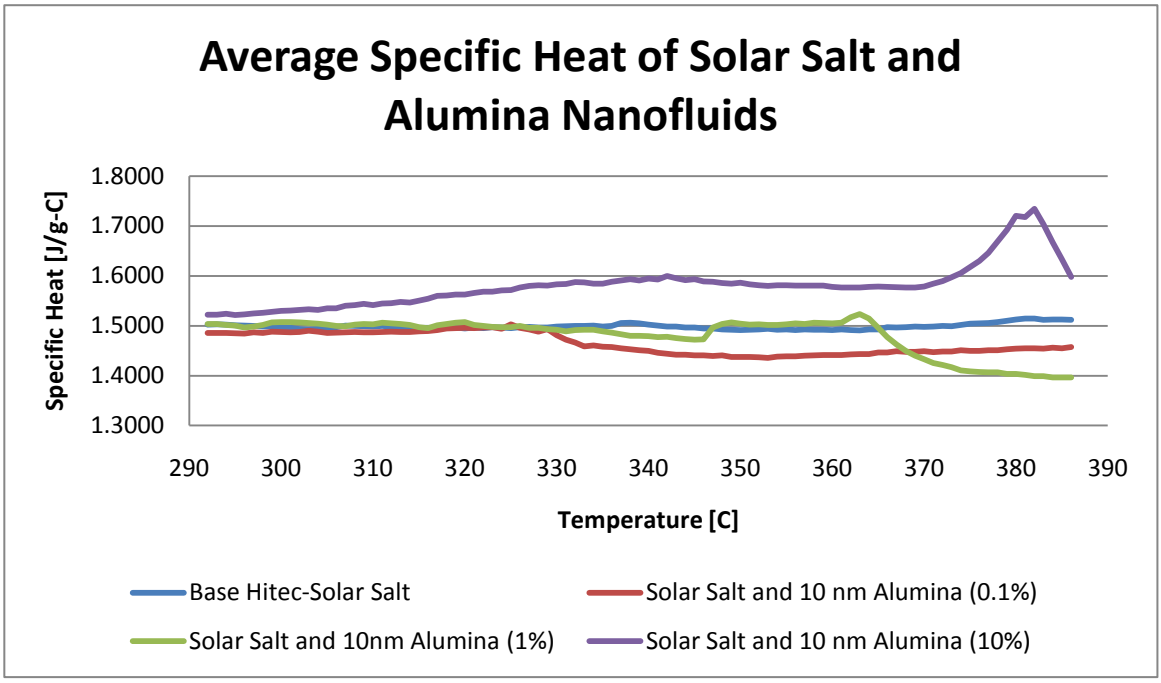

Fig. 25 Mean specific heat values for the Hitec-Solar Salt base fluid as well as the three tested high temperature nanofluids.

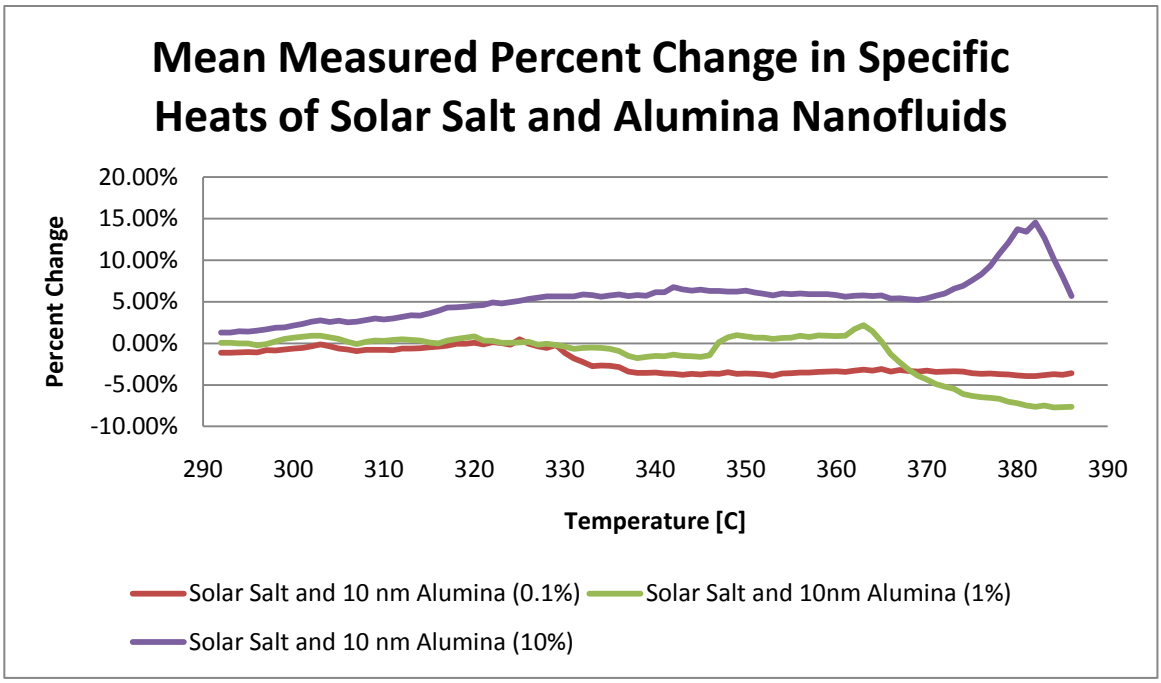

Fig. 26 Percent change in the mean specific heat values, with respect to the Hitec-Solar Salt base fluid, for the three high temperature nanofluids.

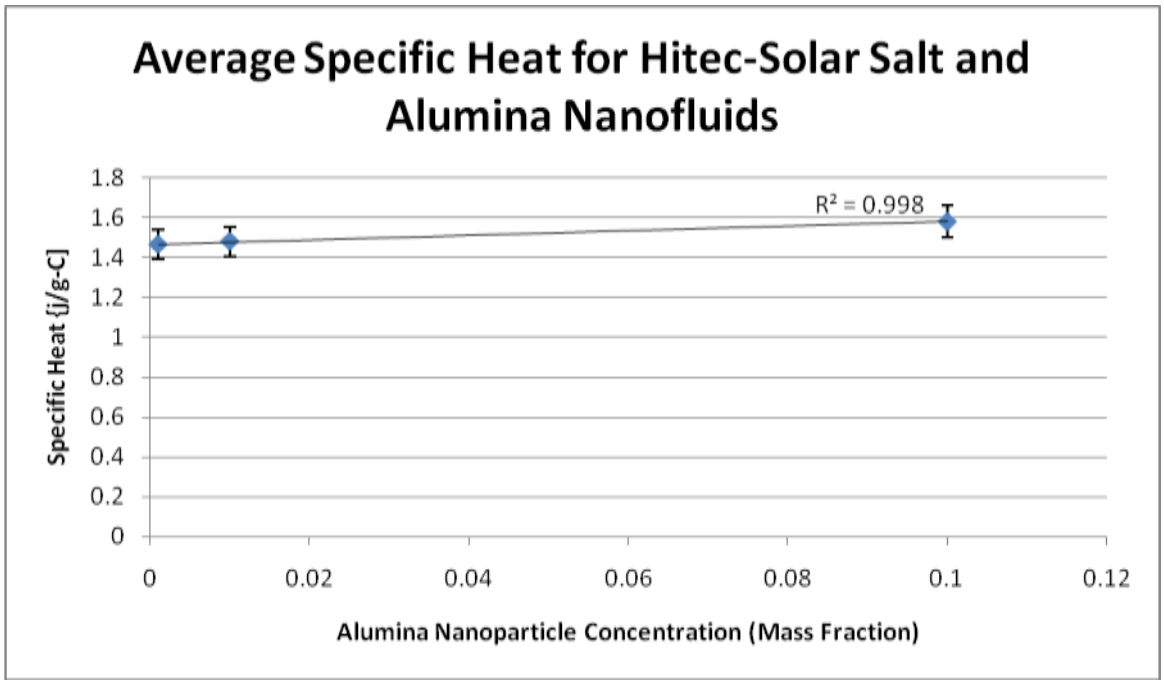

Fig. 27 Correlation between nanoparticle concentration and the specific heat of the prepared high temperature nanofluids.

Despite the strong correlation between the Andasol 1 average specific heat and alumina nanoparticle concentration, the majority of data collected for over the course of this work is statistically inconclusive. Both the 0.1 and 1% alumina nanofluids had sample means which fell within the 90% confidence interval for the Hitec-Solar Salt base fluid. The 10% alumina nanofluid had a sample mean which was higher than the 90% confidence interval for the Hitec-Solar Salt base fluid, Fig. 28.

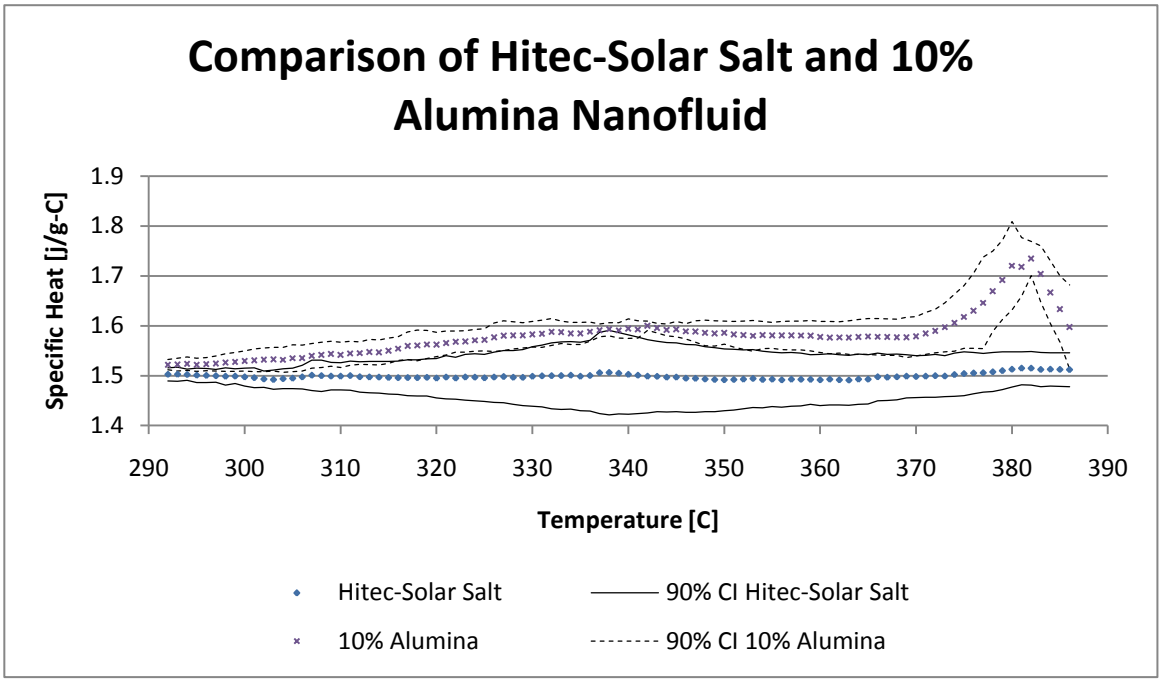

Fig. 28 Mean specific heat and confidence intervals for the Hitec-Solar Salt base fluid and the Hitec-Solar Salt and Alumina (10% conc.) nanofluid.

Traditionally, specific heat capacity increases with temperature. This behavior was observed in the Hitec-Solar Salt base fluid, but was not observed in the high temperature nanofluids. Each of the nanofluids saw a peak in specific heat capacity before the Andasol I 386 ˚C upper temperature limit, which was followed by a decrease in the measured specific heat. The onset of this decrease in specific heat occurred at different temperatures, and therefore different times, for each of the different nanofluids. A linear relationship between the nanoparticle concentration and the onset of the decrease in specific heat was established by taking the natural log of the nanoparticle concentration, Fig. 29.

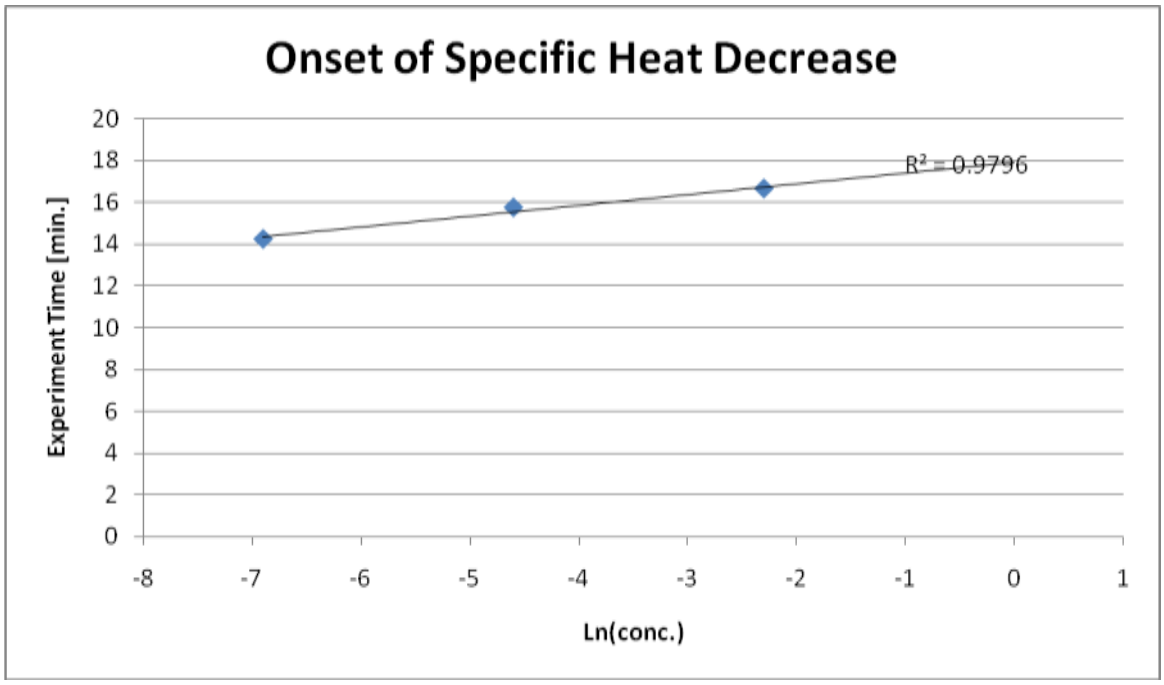

Fig. 29 Correlation between nanoparticle concentration and the onset time of the measured nanofluid specific heat decline.

This relationship is important because it points to the potential instability of the created nanofluids. When all of the available specific heat data is analyzed, it is interesting to note that at higher temperatures, i.e. longer time intervals, the specific heat of nanofluids decreases below that of the base Hitec-Solar Salt. There is currently no explanation for this behavior. If the nanoparticles were simply falling out of solution, one would expect the specific heat of the nanofluids to decrease to that of the base Hitec-Solar Salt. The instability of the nanofluids is something that will have to be addressed if nanofluids are to be used in future thermal energy storage systems.

3.3 Evaluation of Present Specific Heat Models

In addition to characterizing the specific heat of the Hitec-Solar Salt and alumina nanofluids for the purpose of thermal energy storage, this research attempts to expand the current base of

scientific and engineering knowledge by comparing existing nanofluid specific heat models to the experimental results obtained during the characterization of these novel high temperature nanofluids. As discussed in Section 1.3.1 on pg. 14, Zhou analyzed two separate models meant to predict the specific heat of nanofluids. The first model, Eq. 10, was used by Pak to predict the specific heat of water and alumina nanofluids in 1995 [13]. In 2008, Zhou found that the model given in Eq. 11 offered a more accurate prediction of water and alumina nanofluids [10]. In each of the equations C_p is used to represent specific heat, Φ, volume fraction, and ρ, density. The subscripts, $_{np}$ and $_{bf}$, designate the nanoparticle and base fluid properties respectively.

Model used in Pak to predict the specific heat of nanofluids

$$C_{p,nf} = \Phi C_{p,np} + (1-\Phi) C_{p,bf} \tag{10}$$

Model tested by Zhou against the measured specific heat of alumina and water nanofluids

$$C_{p,nf} = \frac{\Phi \rho_{np} C_{p,np} + (1-\Phi)\rho_{bf} C_{p,bf}}{\Phi \rho_{np} + (1-\Phi)\rho_{bf}} \tag{11}$$

The mean specific heat measurements along with their respective confidence intervals are plotted against the available model predictions for each of the investigated nanofluids. As shown in the subsequent plots, the models agree with each other quite well. There is a 0.01%, 0.14%, and 1.31% difference between the two models for the 0.1%, 1% and 10% nanofluids respectively. Prior to the nanofluids going unstable, the models agree quite well with the experimental data from the 0.1 and 1% alumina nanofluids, Fig. 30 and Fig. 31 respectively. Neither model predicts the increase in specific heat seen in the 10% alumina nanofluid, Fig. 32. The percent error in the model predictions for each of the measured nanofluids is given in Table 9.

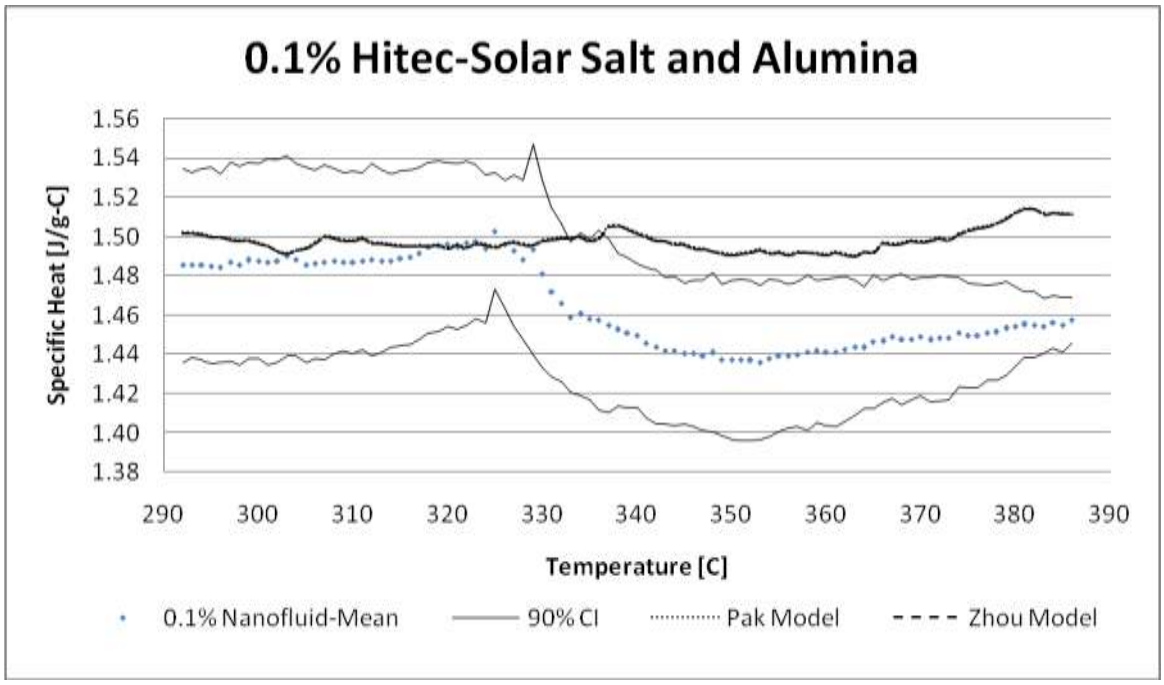

Fig. 30 Model predictions and mean specific heat values for the 0.1% alumina nanofluid.

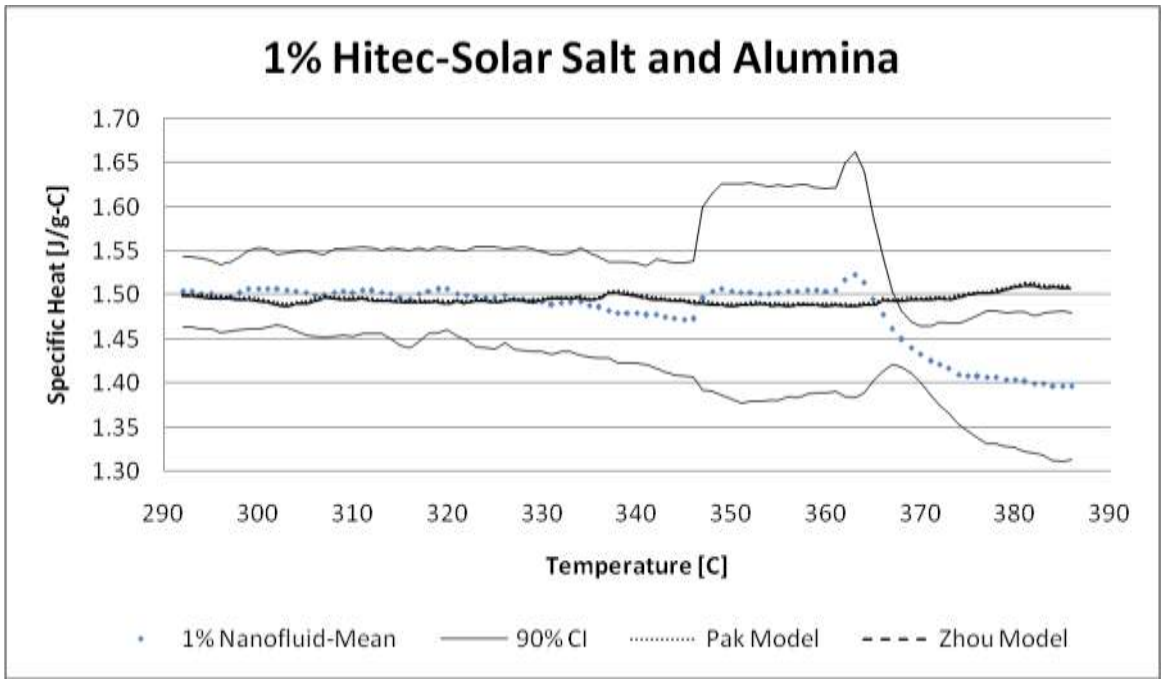

Fig. 31 Model predictions and mean specific heat values for the 1% alumina nanofluid.

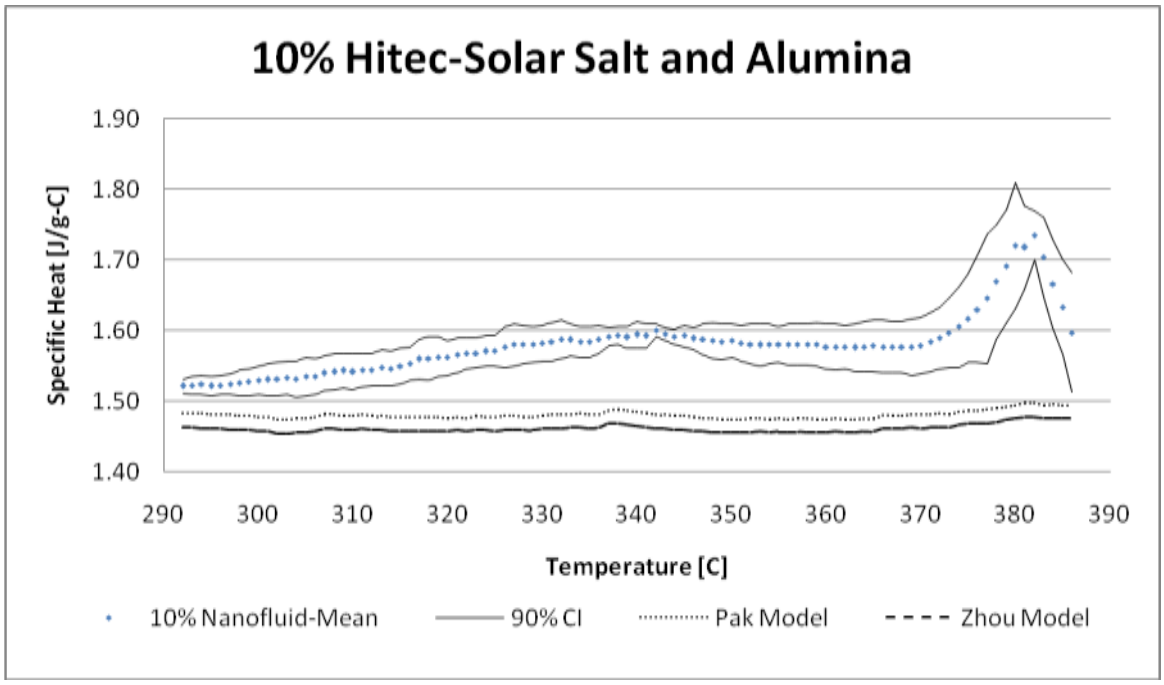

Fig. 32 Model predictions and mean specific heat values for the 10% alumina nanofluid.

Table 9
Percent error in model predictions.

Alumina Conc.	Pak Model	Zhou Model
0.1 %	2.27%	2.24%
1 %	0.96%	1.09%
10 %	-7.52%	-6.72%

It is also important to note that Pak used Eq. 10 (pg. 51) to approximate the specific heat of nanofluids without directly measuring the specific heat of his created nanofluids [13], while Zhou excluded more than 70% of the data he collected:

> *Below 20 °C, a large error occurred because the instrument was still in the transient heating state. At larger temperature, the data are in*

> *relative scatter too. We preferred to measure the average specific heat cp in the temperature range between 25 and 40 °C.* [11]

Zhou's DSC runs spanned a 5-80 ˚C temperature range, for which he utilized a 30 minute isotherm at 5 °C followed by a 25 ˚C/min dynamic heating to 80 ˚C [13]. As shown in Fig. 29 on page 50, it is possible that the nanoparticles began falling out of solution before Zhou began collecting specific heat data over the dynamic heating segment of his DSC measurements. The decrease in specific heat observed by Zhou is consistent with the results seen here in which the specific heat of the nanofluids decreased below that of the base fluid after the nanoparticles began falling out of solution. Additionally, agglomeration and settling of the nanoparticles was observed in the 1% and 10% alumina and Solar Salt nanofluids prepared for the current experiments. It is difficult to believe that Zhou was able to produce stable 21.7% (by volume) alumina-and water nanofluids.

It is possible that the settling of nanoparticles in Zhou's experiments as well as this one resulted in artificially lower specific heat measurements. Previously, nanofluids have been observed to demonstrate improved heat transfer coefficients with respect to their constituent base fluid [20-21]. It is possible that this improvement might be attributable to the tendency of nanoparticles to deposit onto the heat transfer surface creating nanofins which led to better heat transfer between the heat transfer surface and the nanofluid [22-23]. If a similar behavior occurred in the crucibles used by Zhou during his DSC, runs it would result in a lower required differential energy input and ultimately a lower calculated specific heat for the measured nanofluids.

Regardless of the potential deficiencies in previous specific heat experiments, neither model predicted the observed specific heat increase in the 10% alumina and Solar Salt nanofluid.

Both models are essentially averaging schemes which do not account for the molecular reorganization which is believed to lead to the increased specific heat seen in the 10% alumina nanofluid. This potential reorganization of base fluid molecules around the alumina nanoparticles is something that should be investigated in the future but is beyond the scope of the current course of study.

3.4 Discussion of the Full Data Set

As discussed previously, the created high temperature nanofluids were characterized using DSC measurements taken over a 250 to 450 ˚C temperature range with the intent of evaluating the data over the 292 to 386 ˚C temperature range of the Andasol 1 TES system. The percent increase in specific heat over the full 250 to 450 ˚C range is presented in Fig. 33. As shown in Fig. 33, the 1% alumina and Hitec-Solar Salt nanofluid shows a significant improvement in specific heat during the initial stages of the DSC measurement. This peak in specific heat was seen in all three of the 1% alumina and Hitec-Solar Salt samples which were measured in the DSC, see Appendix A.

The mean of the three sample measurements had an approximately 75% improvement in the peak specific heat capacity. The decrease in specific heat capacity is attributed to the proposed instability of the alumina nanoparticles in the liquid Hitec-Solar Salt. These results would suggest that there is an ideal nanoparticle concentration at which significant improvements in the specific capacity can be realized. It is also interesting to note that the onset of nanofluid instability leads to a decrease in minimum specific heat capacity which is correlated with nanoparticle concentration, see Fig. 34.

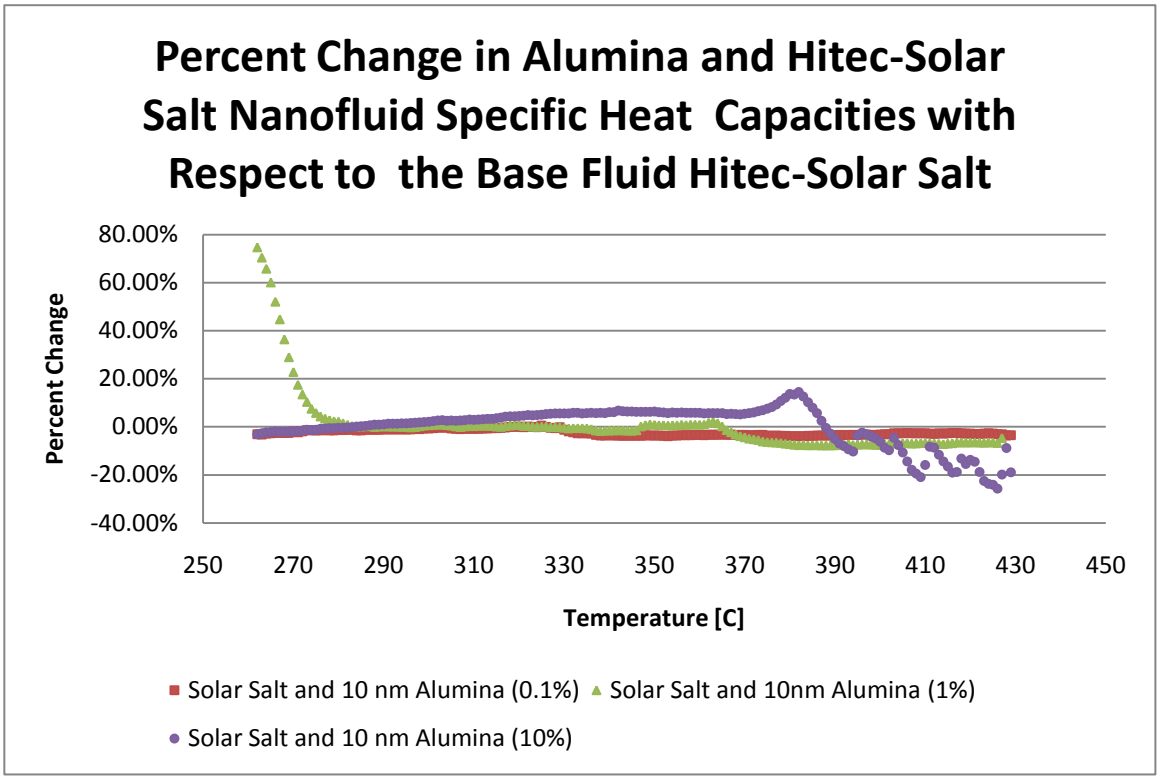

Fig. 33 Percent change in nanofluid specific heat capacity.

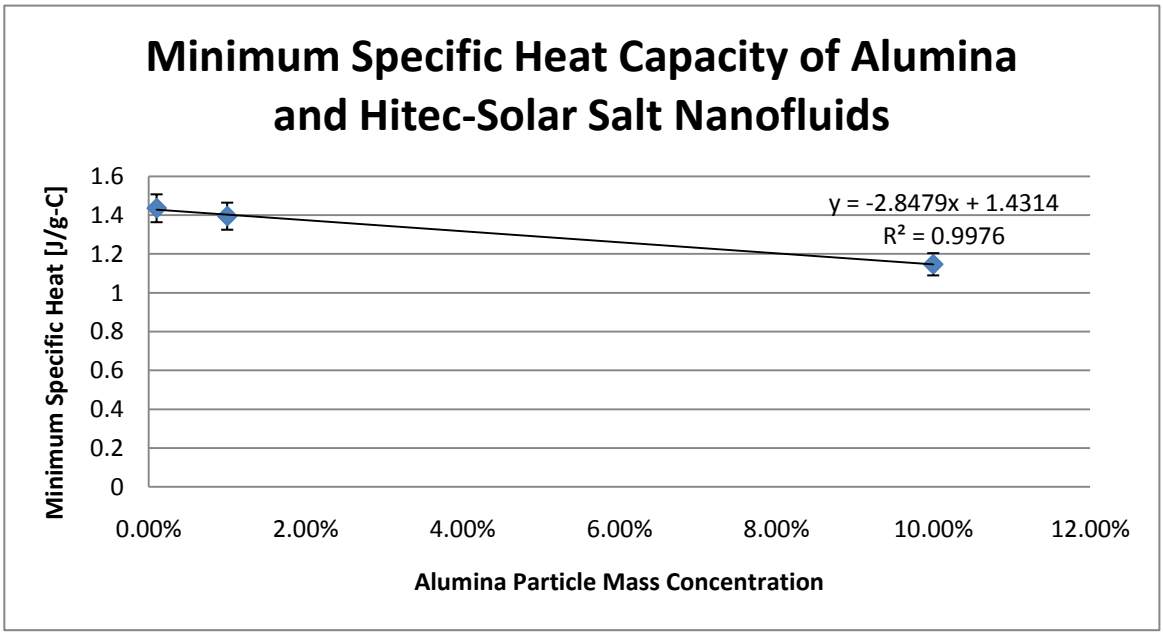

Fig. 34 Correlation between minimum measured specific heat capacity and alumina nanoparticle concentration

The results in Fig. 34 are not meant to contradict the positive correlation between Andasol 1 average specific heat capacity and nanoparticle concentration shown in Fig. 27 on page 48. Instead, the data is meant to support the theory that the lower specific heats measured by Zhou might be the result of nanoparticles falling out of solution and creating nanofins on the crucible surface.

If nanofins are being created on the crucible surface, it stands to reason that nanofluids with higher concentrations of nanoparticles would result in a higher density or larger number of nanofins being produced on the crucible walls. The presence of more nanofins along the crucible surfaces would produce a larger perceived drop in specific heat capacity due to the unaccounted for geometry changes in the experiment apparatus. The production of nanofins or an interconnecting network of nanoparticles during the experiment would explain the decrease in the percent change in specific heat capacity at higher temperatures seen in Fig. 33.

The effect of the nanofins and/or interconnecting networks would be two fold. First, the fins would represent a physical difference between sample and reference crucibles not captured by the baseline measurement. Additionally, these fins have the potential for improving the heat transfer between the crucible and nanofluids which would result in a lower DSC signal and ultimately a lower calculated nanofluid specific heat capacity.

3.5 Nanofluid Geometry Changes

In an effort to determine if geometry changes in the nanofluid may have caused the decline in nanofluid specific heat during the course of the DSC runs, samples of the nanofluid were imaged using scanning electron microscopy, SEM, by members of the DOE project research team. A false color SEM image of the 10% alumina nanofluid prior to the DSC run is shown in Fig. 35. A similar image of the 10% alumina nanofluid after the DSC run is shown in Fig. 36.

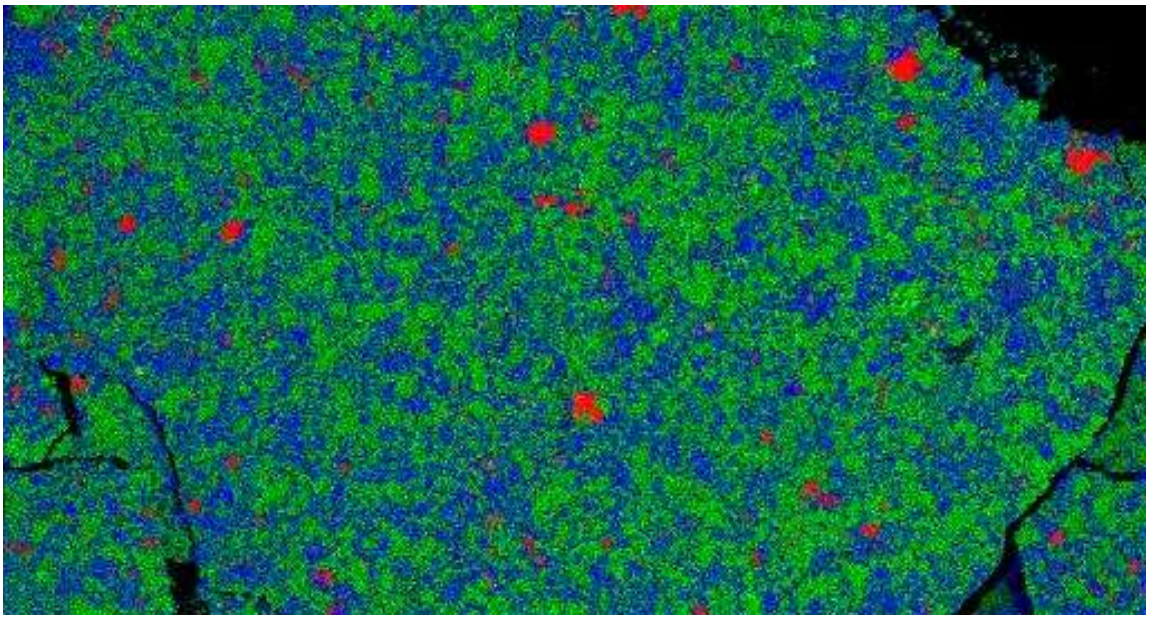

Figure 35 SEM image, provided by Sandhya Shankar, of the unmelted Solar Salt ($NaNO_3$-KNO_3: blue and green respectively) and alumina (pink) 10% concentration nanofluid.

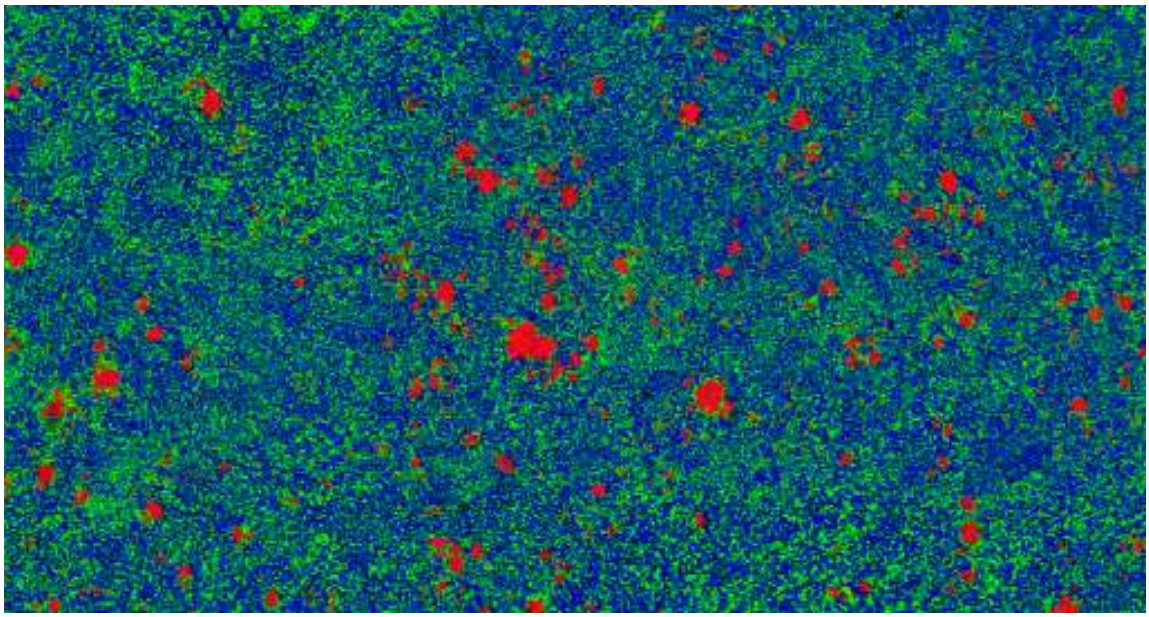

Figure 36 SEM image, provided by Sandhya Shankar, of the melted Solar Salt ($NaNO_3$-KNO_3: blue and green respectively) and alumina (pink) 10% concentration nanofluid.

The images show that a significant amount of agglomeration has occurred during the DSC run. Prior to the DSC run, most of the alumina nanoparticles are smaller than the resolution of

the SEM images. After the DSC run large clusters of the alumina are clearly present. This agglomeration of alumina nanoparticles provides further evidence that these nanofluids are unstable. Imaging of the platinum crucibles used during the DSC run may reveal that these clusters of alumina have fallen out of solution and become plated on the crucible. However, these images are not available at this time.

3.6 Summary of Findings

The investigation of alumina and Hitec-Solar Salt nanofluids has resulted in several findings which have been discussed above and are summarized below.

- Introduction of nanoparticles results in nanofluids which demonstrate specific heat capacities that are higher than the specific heat capacity of the base fluid

- Nanoparticle concentration and Andasol 1 average specific heat capacity are positively correlated

- The current specific heat models fail to accurately predict the measured increase in nanofluid specific heat capacity

- Alumina and Hitec-Solar Salt nanofluids appear to be unstable

- Thermal or temporal instability of the nanofluids cause the measured nanofluid specific heat to decrease below the specific heat of the base fluid

- Nanoparticle concentration and minimum measured specific heat capacity are negatively correlated

These findings led to the conclusions regarding the potential use of nanofluids in thermal energy storage systems which are presented in the following section. In addition to supporting the conclusions presented in Section 4.1, these findings also demonstrate the need for further investigation into the development of high temperature nanofluids. Recommendations for further work in this area are presented in Section 4.2

4. CONCLUSIONS AND RECOMMENDATIONS FOR FUTURE WORK

4.1 Evaluation of the Potential for the Investigated Nanofluids to Impact TES Systems

The strong positive correlation between nanoparticle concentration and nanofluids specific heat proves, with 90% confidence, that it is possible to increase in specific heat of thermal energy storage materials via the introduction of nanoparticles. These findings are contrary to the current theoretical models which fail to account for the potential molecular interaction of the dispersed nanoparticles and the base fluid and suggest that newer models which account for this behavior need to be developed.

The investigated alumina and Solar Salt nanofluids do not offer any cost savings over the current Hitec-Solar Salt TES material. The 0.1% and 1% nanofluids did not demonstrate a statistically significant difference with the specific heat measured for the Hitec-Solar Salt. The 10% nanofluids showed a 5.5% specific heat improvement over the base TES material, but the predicted 89% increase in material cost rules out the potential use of this nanofluid in a TES system.

In addition to the aforementioned material cost issues, the current nanofluids appear to be unstable. The pH of Solar Salt is 6, which is near the equipotential point mentioned in Pak, at which alumina nanoparticle agglomeration and settling occur [13]. Thermal energy storage systems are required to operate for years at a time and require stable TES materials. Potentially, more stable high temperature nanofluids could be created through the use of different nanoparticles or pH doping the Hitec-Solar Salt. Additionally, the pumps used to transport the fluid from one tank to the next or through the solar field could be used to provide turbulent mixing of the TES material; however, the cost of this type of mixing system would need to be investigated.

Solving the nanofluid stability problem is of utmost importance. The expanded DSC data shows that a 75% improvement in specific heat was observed briefly for the 1% alumina and Solar Salt nanofluid. If this improvement could be maintained throughout the operation of a TES system, it would create a potential 37% costs savings over the current Hitec-Solar Salt thermal energy storage material.

4.2 Recommendations for Future Work

The observed decrease in nanofluid specific heat suggests that the created nanofluids are either temporally or thermally unstable. The source of this instability needs to be quantified before potential solutions can be identified. DSC measurements could be performed at faster and/or slower heating rates as a means of trying to identify the source of this instability. Additionally, the isothermal period before the dynamic heating of the DSC samples could be increased or decreased to determine if time or temperature is the main driver in the current nanofluid instability.

An entirely different set of experiments could be designed to determine the cause of this behavior. These experiments would involve placing the nanofluids into two stainless steel sealed containers which would then be placed in a furnace. Settling of the nanoparticles could be observed by placing one of the containers in a vertical orientation and the other in a horizontal orientation. The samples could then be heated to various temperatures or for various periods of time, depending on the instability source being investigated. Flash freezing of the samples would allow the nanoparticle distribution to be observed via activation analysis or similar technique. The horizontal sample would provide the control sample needed for comparison.

The potential of nanoparticles to produce artificially low specific heat measurements by creating nanofins on the sample crucibles should also be investigated. These nanofins should be

observable via Scanning Electron or Transmission Electron Microscopy (SEM, TEM). Additionally, the stainless steel containers used in the instability tests could double as a means of determining the possibility of this behavior occurring in the tanks and piping of TES systems.

Ultimately, nanofluid stability needs to be improved, and the impact of pH doping the Solar Salt could be observed directly in the DSC, although this may raise corrosion and safety issues which invalidate this approach. A safer approach would be to create nanofluids using different nanoparticles. Silica, unlike titania and alumina, is soluble in water and may be more stable in Hitec-Solar Salt than the currently used alumina nanoparticles.

REFERENCES

[1] G. Ondrey, Solar's second coming, Chemical Engineering 116 (2009) 18-21.

[2] Andasol 1 goes into operation, RenewableEnergyWorld.com (2008) http://www.renewableenergyworld.com/rea/news/article/2008/11/andasol-1-goes-into-operation-54019.

[3] J.T. McKinnon, A primer on CSP, World Watch 21 (2008) p. 29.

[4] U. Hermann, D. Kearney, Survey of thermal energy storage for parabolic trough power plants, ASME J. of Solar Energy Engineering 124 (2002) 145-152.

[5] J.M. Chavez, H.E. Reilly, G.J. Kolb, B. Gould, A. Zavoico, P. Sutherlad, The solar two power tower project: A 10 MWe power plant, Proceedings of the 30th Intersociety Energy Conversion Engineering Conference, Orlando, FL, pp. 469-475.

[6] National Renewable Energy Laboratory, Survey of Thermal Storage for Parabolic Trough Power Plants, NREL/SR-550-27925, National Renewable Energy Laboratory, Golden, CO (2000).

[7] D. Brosseau, J.W. Kelton, D. Ray, M. Edgar, K. Chisman, B. Emms, Testing of thermocline filler materials and molten-salt heat transfer fluids for thermal energy storage systems in parabolic trough power plants, ASME J. of Solar Energy Engineering 127 (1) (2005) 109-116.

[8] K.C. Divya, J. Ostergaard, Battery energy storage technology for power systems – An overview, Electric Power Systems Research 79 (4) (2009) 511-520.

[9] H. Hermman, P. Nava, Thermal energy storage for a 50 MW trough power plant in Spain, Trough Workshop, Lake Tahoe, CA, Feb. 2006.

[10] D. Wen, G. Lin, S. Vafaei, K. Zhang, Review of nanofluids for heat transfer applications, Particuology 7 (2) (2009) 141-150.

[11] S.Q. Zhou, R. Ni, Measurement of the specific heat of water-based AL_2O_3 nanofluid, Applied Physics Letters 92 (9) (2008).

[12] I.C. Nelson, D. Banerjee, Flow loop experiments using nanofluids, Poster Presentation, Texas A&M University, College Station, (2009).

[13] B.C. Pak, Y.I. Cho, Hydrodynamic and heat transfer study of dispersed fluids with submicron metallic oxide particles, Experimental Heat Transfer 11 (2) (1998) 151-170.

[14] ASTM International, Standard test method for determining specific heat capacity by differential scanning calorimetry, ASTM E 1269 (2005).

[15] Netzsch Instruments, NETZSCH Proteus – Thermal Analysis – Version 4.8.4, Netzsch-Geraetebau GmbH (2007).

[16] D. Vuclelic, V. Vucelic, N. Juranic, Quantitative determination of specific heat by differential scanning calorimetry, J. of Thermal Analysis 5 (4) (1973) 459-463.

[17] ASTM International, Standard test method for thermal diffusivity by the flash method, ASTM E 1461 (2007).

[18] Netzsch Instruments, NETZSCH Proteus – LFA Thermal Analysis – Version 4.8.4, Netzsch-Geraetebau GmbH, The Netzsch Group, Selb, Germamy (2007).

[19] Hitec Solar Salt, Coastal Chemical Co., L.L.C. Houston, TX (2009).

[20] X.Q. Wang, A.S. Mujumdar, Heat transfer characterization of nanofluids: A review, International Journal of Thermal Sciences 46 (1) (2007) pp. 1-19.

[21] C.J. Ho, L.C. Wei, Z.W. Li, An experimental investigation of forced convective cooling performance of a microchannel heat sink with Al_2O_3/water nanofluid, Applied Thermal Engineering 30 (2) (2010) 96-103.

[22] R. Chein, J. Chuang, Experimental microchannel heat sink performance studies using nanofluids, International Journal of Thermal Sciences 46 (1) (2007) 57-66.

[23] X. Wu, H. Wu, P. Cheng, Pressure drop and heat transfer of Al_2O_3-H_2O nanofluids through silicon microchannels, J. of Micromechanics and Microengineering 19 (10) (2009) 1-11.

APPENDIX A

HIGH TEMEPERATURE SOLAR SALT AND ALUMINA NANOFLUIDS-SPECIFIC HEAT MEASUREMENTS

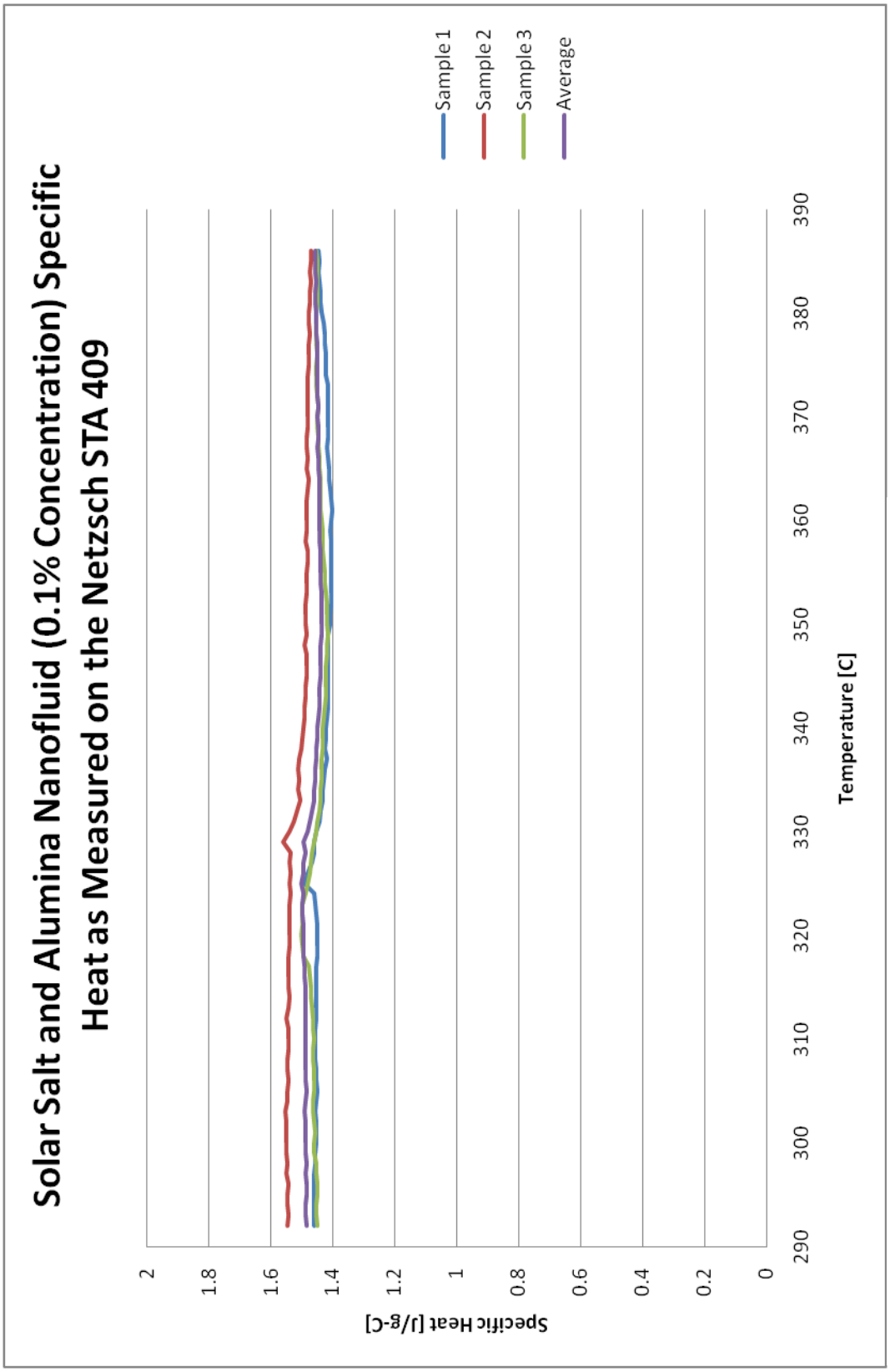

Andasol 1- Solar Salt and 10 nm Alumina 0.1% Mass Concentration

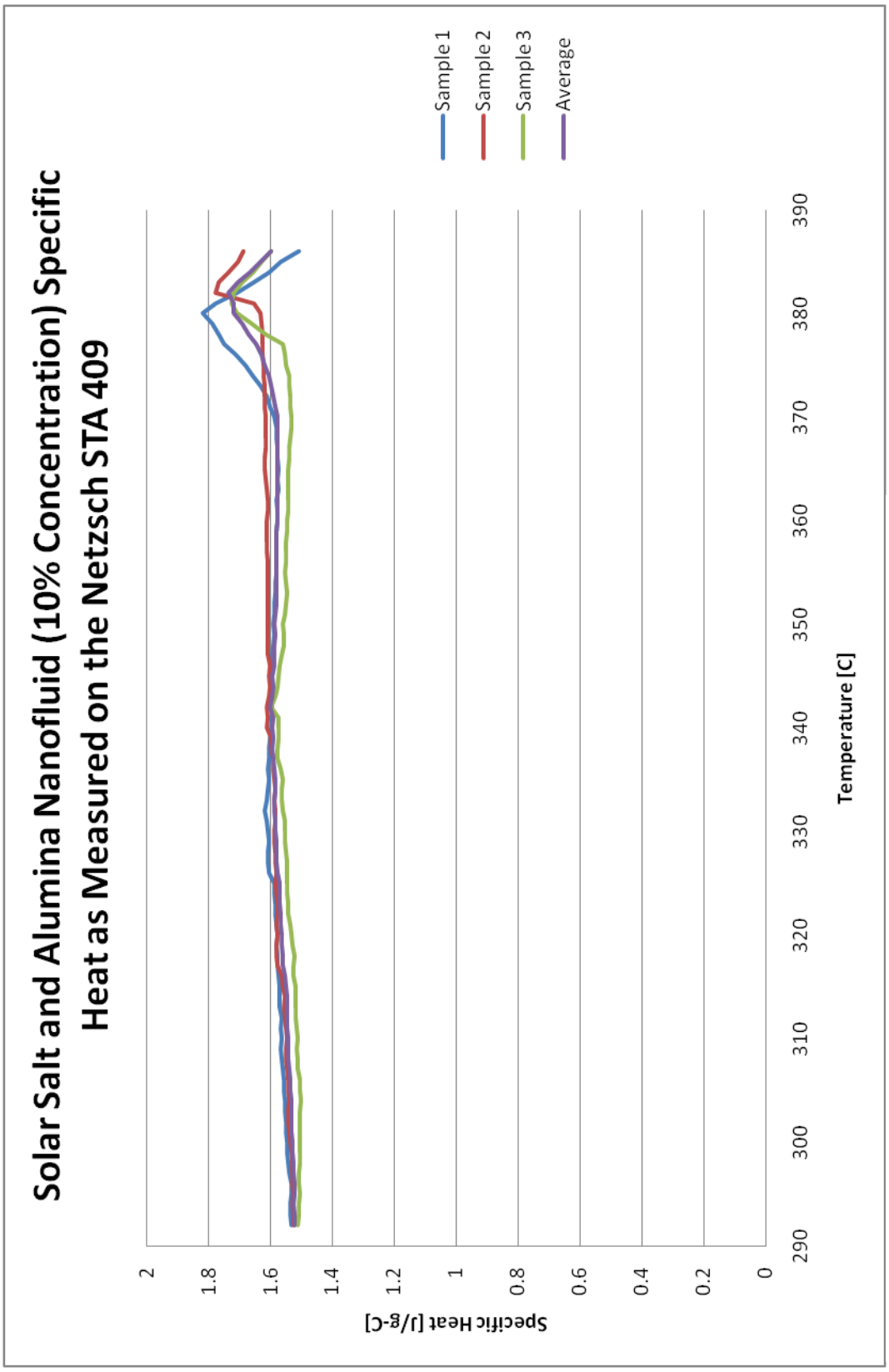

Andasol 1- Solar Salt and 10 nm Alumina 10% Mass Concentration

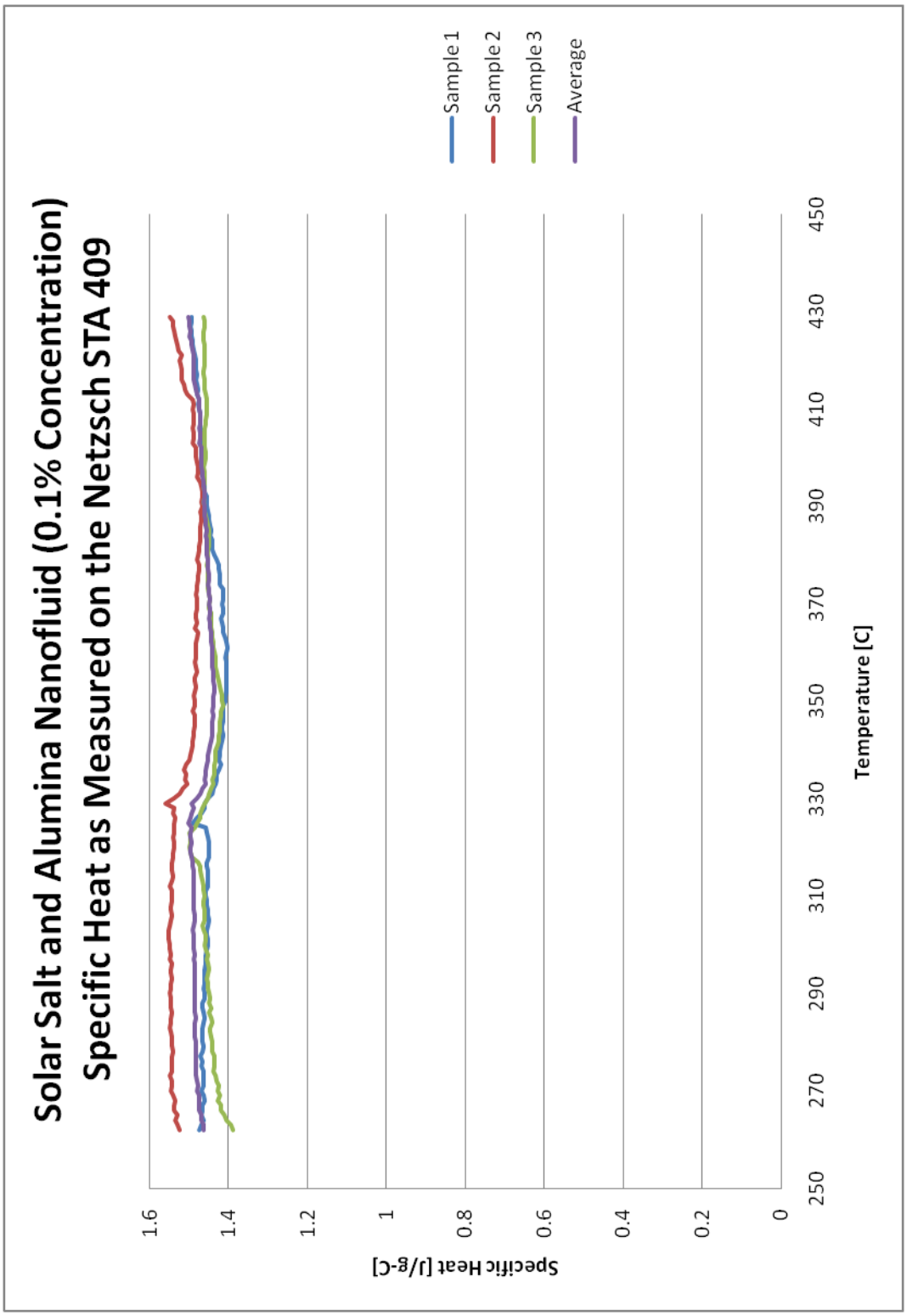

Full Data Set - Solar Salt and 10 nm Alumina 0.1% Mass Concentration

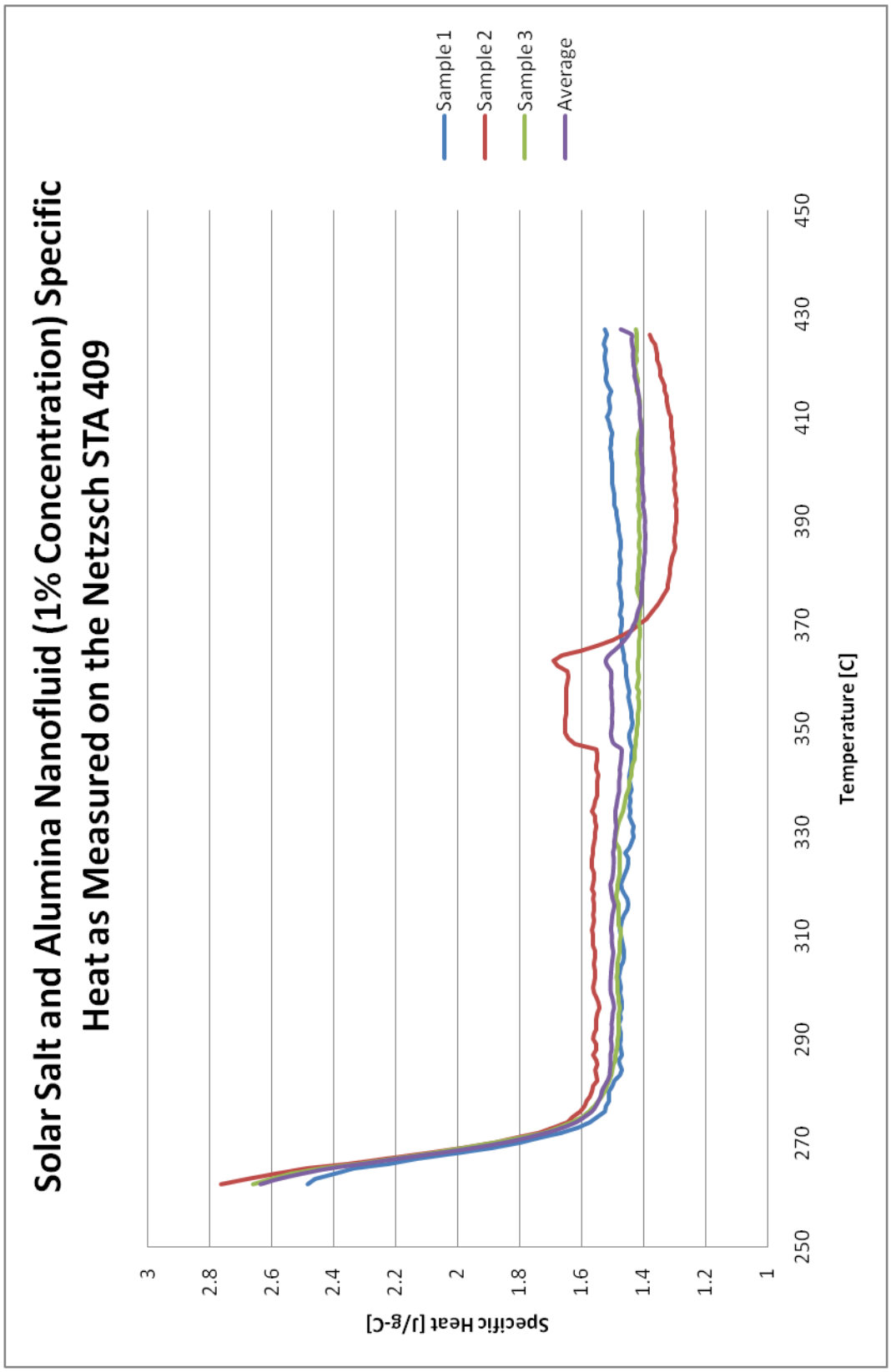

Full Data Set - Solar Salt and 10 nm Alumina 1% Mass Concentration

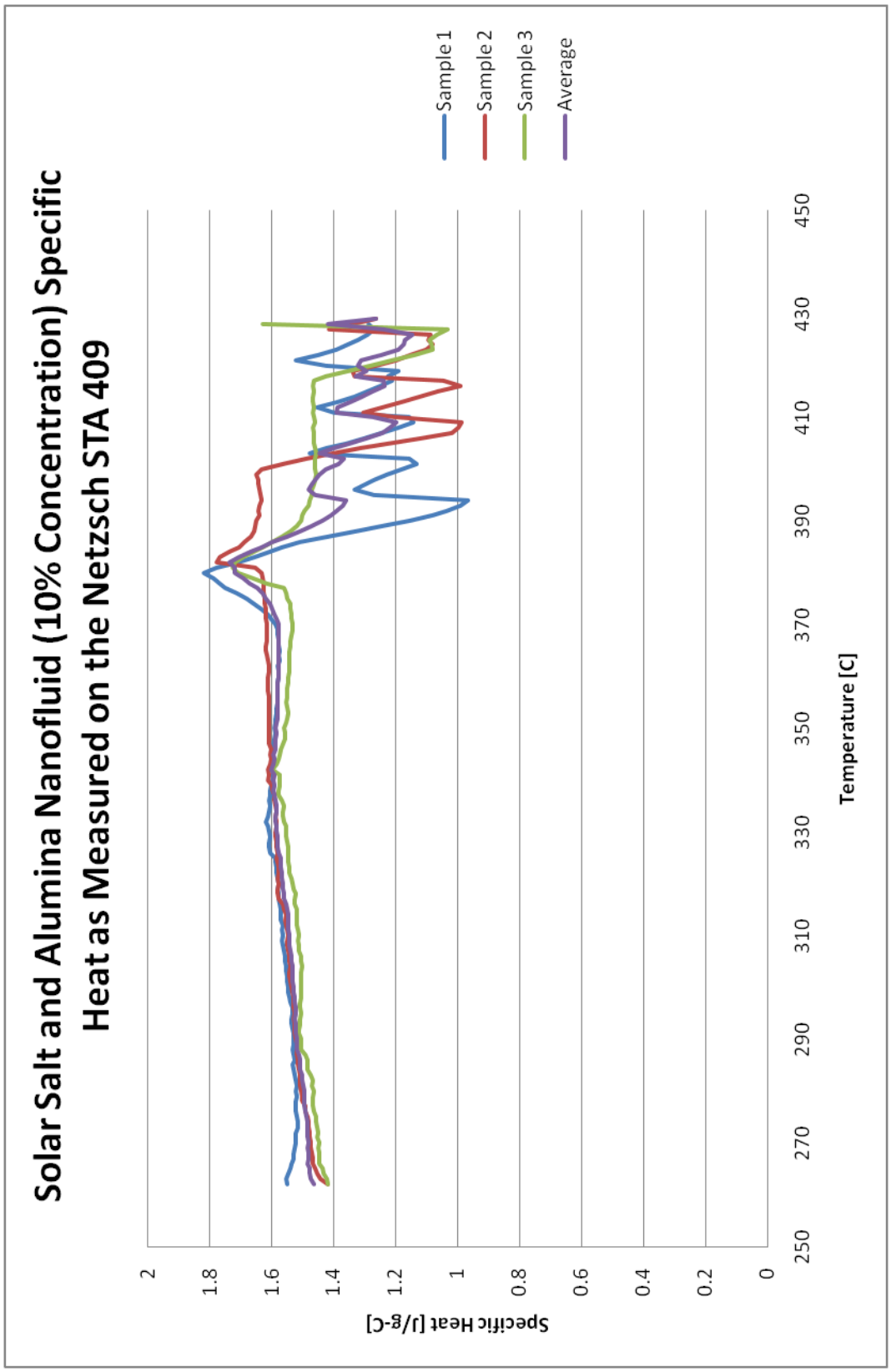

Full Data Set - Solar Salt and 10 nm Alumina 10% Mass Concentration

VITA

Name:	Darren Ross Malik
Address:	3330 Oakwell Court Suite 100, San Antonio, TX 78218
Email Address:	drmalik86@yahoo.com
Education:	B.S., Nuclear Engineering, Texas A&M University, 2008